Doc2b Is a High-Affinity Ca^{2+} Sensor for Spontaneous Neurotransmitter Release

Alexander J. Groffen,[1]*§ Sascha Martens,[2]*†§ Rocío Díez Arazola,[1] L. Niels Cornelisse,[1] Natalia Lozovaya,[1,3,4] Arthur P. H. de Jong,[1] Natalia A. Goriounova,[1,3] Ron L. P. Habets,[5]‡ Yoshimi Takai,[5] J. Gerard Borst,[4] Nils Brose,[6] Harvey T. McMahon,[2]* Matthijs Verhage[1]*

Synaptic vesicle fusion in brain synapses occurs in phases that are either tightly coupled to action potentials (synchronous), immediately following action potentials (asynchronous), or as stochastic events in the absence of action potentials (spontaneous). Synaptotagmin-1, -2, and -9 are vesicle-associated Ca^{2+} sensors for synchronous release. Here we found that double C2 domain (Doc2) proteins act as Ca^{2+} sensors to trigger spontaneous release. Although Doc2 proteins are cytosolic, they function analogously to synaptotagmin-1 but with a higher Ca^{2+} sensitivity. Doc2 proteins bound to *N*-ethylmaleimide–sensitive factor attachment receptor (SNARE) complexes in competition with synaptotagmin-1. Thus, different classes of multiple C2 domain–containing molecules trigger synchronous versus spontaneous fusion, which suggests a general mechanism for synaptic vesicle fusion triggered by the combined actions of SNAREs and multiple C2 domain–containing proteins.

Neurotransmitter release is triggered by a rise in intracellular Ca^{2+}, which activates sensors that subsequently trigger vesicle fusion. Synchronous release, the fastest mode of neurotransmission, involves the Ca^{2+} sensors synaptotagmin-1, -2, or -9, which are anchored in the vesicle membrane and contain two cytoplasmic C2 domains that bind phospholipids in a Ca^{2+}-dependent manner and interact with the soluble *N*-ethylmaleimide–sensitive factor attachment receptor (SNARE) complex (*1*–*5*). Synaptotagmin-1–deficient neurons lack synchronous release but display an increase in spontaneous release (*6*–*9*) except in autapses (*1*, *10*), which suggests a distinct mechanism for spontaneous release. Spontaneous release occurs in the absence of action potentials and is largely Ca^{2+} dependent (*11*–*15*), although truly Ca^{2+}-independent fusion may also exist (*16*).

Doc2a and Doc2b are soluble proteins that contain C2 domains, which are similar to synaptotagmins (*17*, *18*). They are expressed in nerve terminals and interact with the secretory molecules Munc18 and Munc13 and the SNARE proteins syntaxin-1 and SNAP25 (the synaptosome-associated protein of 25 kD) (*19*, *20*). Overexpression of Doc2b enhances exocytosis in chromaffin cells

[1]Department of Functional Genomics, CNCR, Neuroscience Campus Amsterdam, VU University and VU Medical Center, Amsterdam, 1081 HV, Netherlands. [2]Medical Research Council (MRC) Laboratory of Molecular Biology, Hills Road, Cambridge, CB2 0QH, UK. [3]Department of Integrative Neurophysiology, CNCR, VU University, Amsterdam, 1081 HV, Netherlands. [4]Bogomoletz Institute of Physiology, Kiev, 01024, Ukraine. [5]Department of Neuroscience, Erasmus MC, University Medical Center, Rotterdam, 3000 CA, Netherlands. [6]Department of Biochemistry and Molecular Biology, Kobe University Graduate School of Medicine, Kobe 650-0017, Japan. [7]Max-Planck-Institut für Experimentelle Medizin, Abteilung Molekulare Neurobiologie, 37075 Göttingen, Germany.

*These authors contributed equally to this work.
†Present address: Max F. Perutz Laboratories, University of Vienna, Dr. Bohr-Gasse 9/3, 1030 Vienna, Austria.
‡Present address: Department of Molecular and Developmental Genetics, K.U.Leuven, Center for Human Genetics, 3000 Belgium.
§To whom correspondence should be addressed. E-mail: sander.groffen@cncr.vu.nl (A.J.G.) and sascha.martens@univie.ac.at (S.M.)

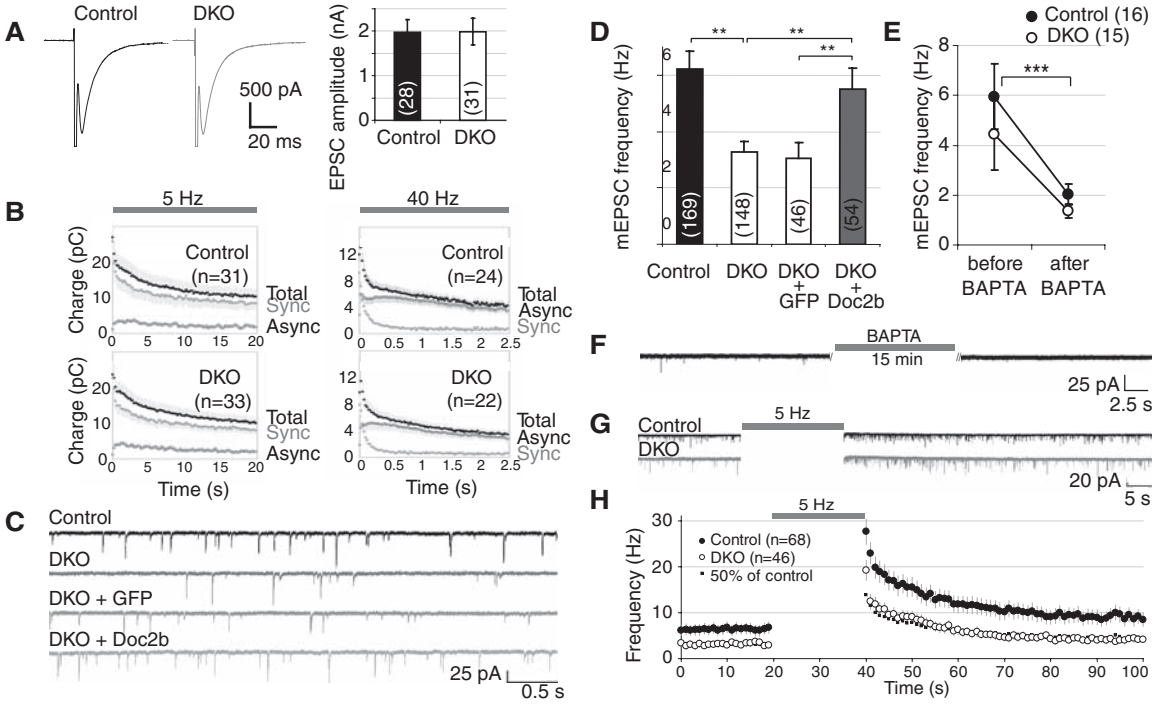

Fig. 1. Impaired spontaneous neurotransmission in Doc2a- and b-deficient mice. Hippocampal neurons were cultured on microislands to promote self-innervation. (**A**) Averaged evoked EPSCs in control and DKO neurons. (**B**) Evoked EPSC charge (mean ± SEM) during repeated stimulation at 5 or 40 Hz. The synchronous and asynchronous components were estimated as previously reported (*25*). (**C**) Representative traces of spontaneous EPSCs in wild-type or DKO cells. To rescue the phenotype, GFP or Doc2b was acutely expressed in DKO cells. (**D**) Average spontaneous release frequency in control and DKO cells and rescue by Doc2b overexpression. Cell numbers are indicated between brackets. $^{**}P < 0.01$. (**E**) Average mEPSC frequency before and after intracellular loading of the Ca^{2+} chelator BAPTA. The average spontaneous release rate varied between experiments, but our experimental design prevents confounding effects thereof (fig. S2E) (**F**) Example trace representative for the data in (E), taken from a DKO cell before and after BAPTA loading. (**G**) Typical recordings before and after repetitive stimulation at 5 Hz. (**H**) Individual release events were binned in 1-s time intervals to monitor their average frequency immediately after repetitive stimulation. Squares were calculated as 50% of the frequency in control cells.

(*19*), pancreatic beta cells (*21*, *22*), and adipocytes (*23*), but its function in neurons is elusive.

Role of Doc2b and Ca^{2+} in spontaneous synaptic release. We generated *Doc2b*$^{-/-}$ mice by deleting the promoter and exon 1 of the *Doc2b* gene (fig. S1) (*24*). *Doc2b*$^{-/-}$ mice did not express the remaining exons and lacked Doc2b immunoreactivity. *Doc2b*$^{-/-}$ mice were viable and fertile without gross abnormalities. Other proteins implicated in neurotransmitter secretion were expressed at normal levels (fig. S1D). Compensatory ectopic expression of *Doc2a* was not detected in Doc2b-deficient brains by in situ hybridization and the Doc2a protein level was unchanged (fig. S1). *Doc2a*$^{-/-}$ *Doc2b*$^{-/-}$ double knock-out (DKO) mice were also viable, fertile, and indistinguishable with regard to gross anatomy. To study neurotransmission and synaptic plasticity in Doc2 mutants, hippocampal neurons were cultured on glial microislands to promote self-innervation (autapses). Because Doc2a and Doc2b are both expressed in the hippocampus (*18*), DKO mice were compared with wild-type controls. All aspects of evoked release were normal, with excitatory postsynaptic currents (EPSCs) of normal amplitude and shape (Fig. 1A), a normal synaptic depression during prolonged stimulation at 5 or 40 Hz (Fig. 1B and fig. S2, A and B), a normal contribution to the total postsynaptic charge transfer (*25*) of asynchronous release (Fig. 1B) and a normal size of the readily releasable pool (RRP) (fig. S2D).

However, DKO mice exhibited a reduction in the spontaneous release frequency to half that of controls (6.2 Hz in wild type to 3.3 Hz in DKO) (Fig. 1, C and D). Acute expression of Doc2b in DKO neurons restored this phenotype. Doc2b immunoreactivity was confirmed in all cellular compartments, including synapses, at the time of analysis (fig. S3). As a control, acute expression of green fluorescent protein (GFP) in DKO cells did not affect the spontaneous release frequency (3.1 Hz) (table S1). A normal organization of the postsynaptic apparatus was indicated by a normal miniature EPSC (mEPSC) amplitude, as well as normal rise time and decay time in DKO neurons (fig. S2F) or after overexpression (fig. S3B).

Because Doc2 proteins require Ca^{2+} for their phospholipid-binding and secretion-enhancing activity (*19*, *26*), we investigated whether spontaneous release also depended on Ca^{2+}. The spontaneous release frequency was measured in the same cells before and after loading them with the Ca^{2+} che-

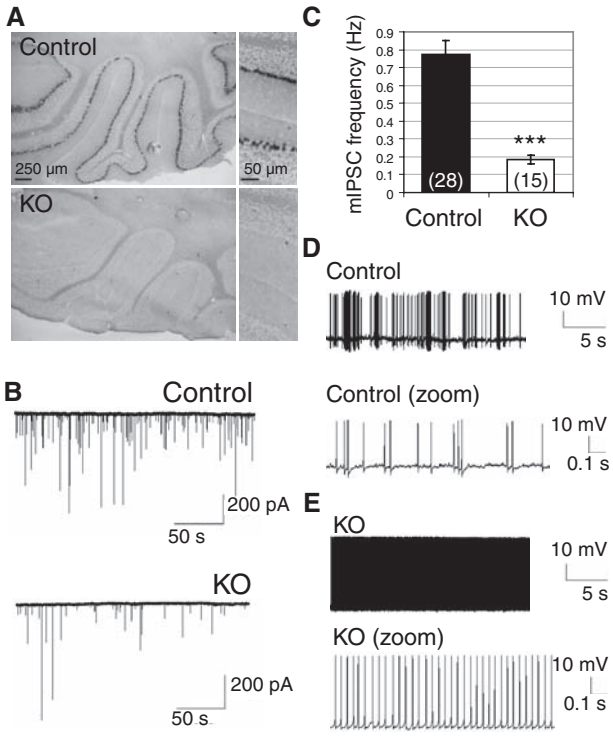

Fig. 2. Reduced frequency of spontaneous events in Purkinje cells lacking Doc2b. (**A**) Doc2b mRNA was detected by in situ hybridization in cerebellar Purkinje cells from wild-type, but not *Doc2b*$^{-/-}$ (KO) mice. (**B**) Typical voltage-clamp recordings in acute slices. (**C**) Mean frequency of spontaneous miniature inhibitory postsynaptic currents (mIPSCs) in KO mice and age-matched control littermates (n = 15 and 28 cells from two and three mice, respectively). ***$P < 0.0001$. (**D** and **E**) Representative current clamp recordings of Purkinje cell firing patterns in controls (D) (eight cells from three mice) and KO cells (E) (seven cells from two mice).

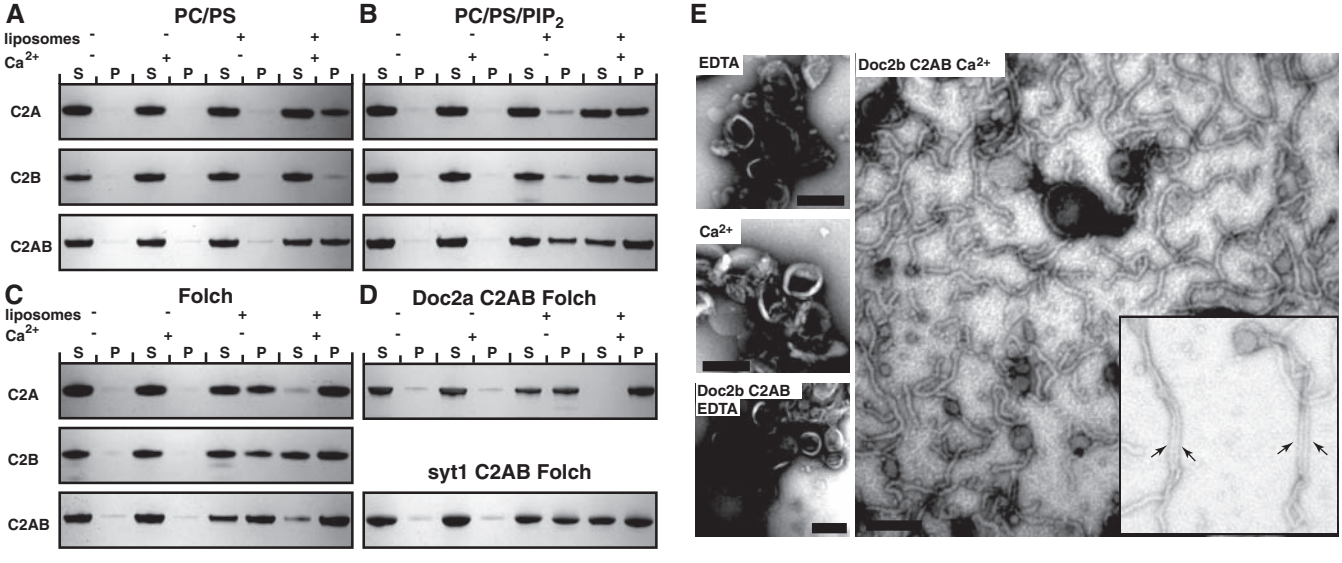

Fig. 3. Membrane-binding and curvature induction by Doc2b. (**A** to **D**) Liposome cosedimentation assays to characterize the membrane-binding properties of the Doc2b C2A, C2B, C2AB, Doc2a C2AB, and synaptotagmin-1 (Syt1) C2AB domains. Liposomes composed of the indicated lipids were incubated with the Doc2b C2A, C2B, or C2AB domains. Liposome-bound protein was cosedimented by ultracentrifugation. Eight percent of the supernatant and of the pellet fraction was run on 4 to 12% gradient gels. Proteins were visualized by Coomassie staining. S indicates unbound protein in the supernatant; P indicates liposome-bound, and thus copelleted, protein. No or very little protein sedimented in the absence of liposomes. (**E**) Ca^{2+}-dependent tubulation of liposomes by the Doc2b C2AB domain. Folch liposomes were incubated in the absence or presence of Doc2b C2AB and/or Ca^{2+} and processed for electron microscopy by negative stain. The arrows indicate bundles of closely aligned tubules. Scale bar, 100 nm. All data shown are representative of at least three independent experiments. PS, phosphatidylserine; PC, phosphatidylcholine.

lator 1,2-bis(2-aminophenoxy)ethane-*N*,*N*,*N*′,*N*′-tetraacetic acid (BAPTA). This significantly reduced the frequency to 2.0 Hz ($P < 0.0001$) in wild-type cells and to 1.4 Hz in DKO cells ($P < 0.0001$) (Fig. 1, E and F). The frequency did not decrease further after longer incubation with BAPTA-AM (a membrane-permeable form of BAPTA) (fig. S2H). Thus, as expected (*12*–*15*), spontaneous events are often triggered by short-lived Ca^{2+} transients in resting cells.

Consistent with the role of Ca^{2+} in spontaneous release, the frequency of individual release events markedly increased after intense activity (5 Hz for 20 s) (Fig. 1, G and H) and decayed after the last stimulus with an exponential $t_{1/2}$ of 11 s. Similar observations have been made in the neuromuscular junction and calyx of Held (*27*, *28*). In DKO cells after intense stimulation, the number of observed events was reduced to 50% of wild type, except for the first time point that was sampled 200 to 1200 ms after the last depolarizing stimulus, where asynchronous release may still contribute (Fig. 1H). The Doc2-independent events remaining in DKO cells were also affected by BAPTA and repetitive firing, which suggested that additional Ca^{2+}-dependent mechanisms exist besides Doc2a- and b-dependent events. Thus Doc2 proteins responding to intracellular Ca^{2+} are required for approximately half of the spontaneous release events in hippocampal neurons.

Disinhibition in Purkinje cells lacking Doc2b. *Doc2b* mRNA was abundant in Purkinje cells (PCs) of the cerebellum (Fig. 2A), whereas *Doc2a* was not detectable. *Doc2b* expression was exclusive to the PC layer with no detectable mRNA in other cerebellar cells including interneurons. PCs synapse onto neighboring PCs via recurrent axon collaterals (*29*). We performed whole-cell voltage-clamp recordings at postnatal days 7 to 8 because at this time, recurrent synapses are the predominant source of GABA-mediated (GABAergic) input, whereas stellate and basket cells are still functionally immature (*30*). In the presence of 6,7-dinitroquinoxaline-2,3-dione (DNQX) to block AMPA receptors and tetrodotoxin (TTX) to block sodium currents, the PCs had a stable resting potential without *N*-methyl-D-aspartate receptor currents or Ca^{2+} spikes. Under these conditions, any remaining inhibitory postsynaptic currents (IPSCs) can be interpreted as spontaneous release events.

The frequency of spontaneous IPSCs was reduced to one-fourth in $Doc2b^{-/-}$ mice compared with control littermates (Fig. 2, B and C). Postsynaptic parameters were normal (i.e., amplitude, rise time, and decay). In young rodents, GABAergic input inhibits PC firing (*30*), and recurrent PC-PC synapses are the major GABA source (*31*). We thus tested if the disinhibition in $Doc2b^{-/-}$ PC-PC synapses affected PC spiking. Whole-cell current clamp recordings were per-

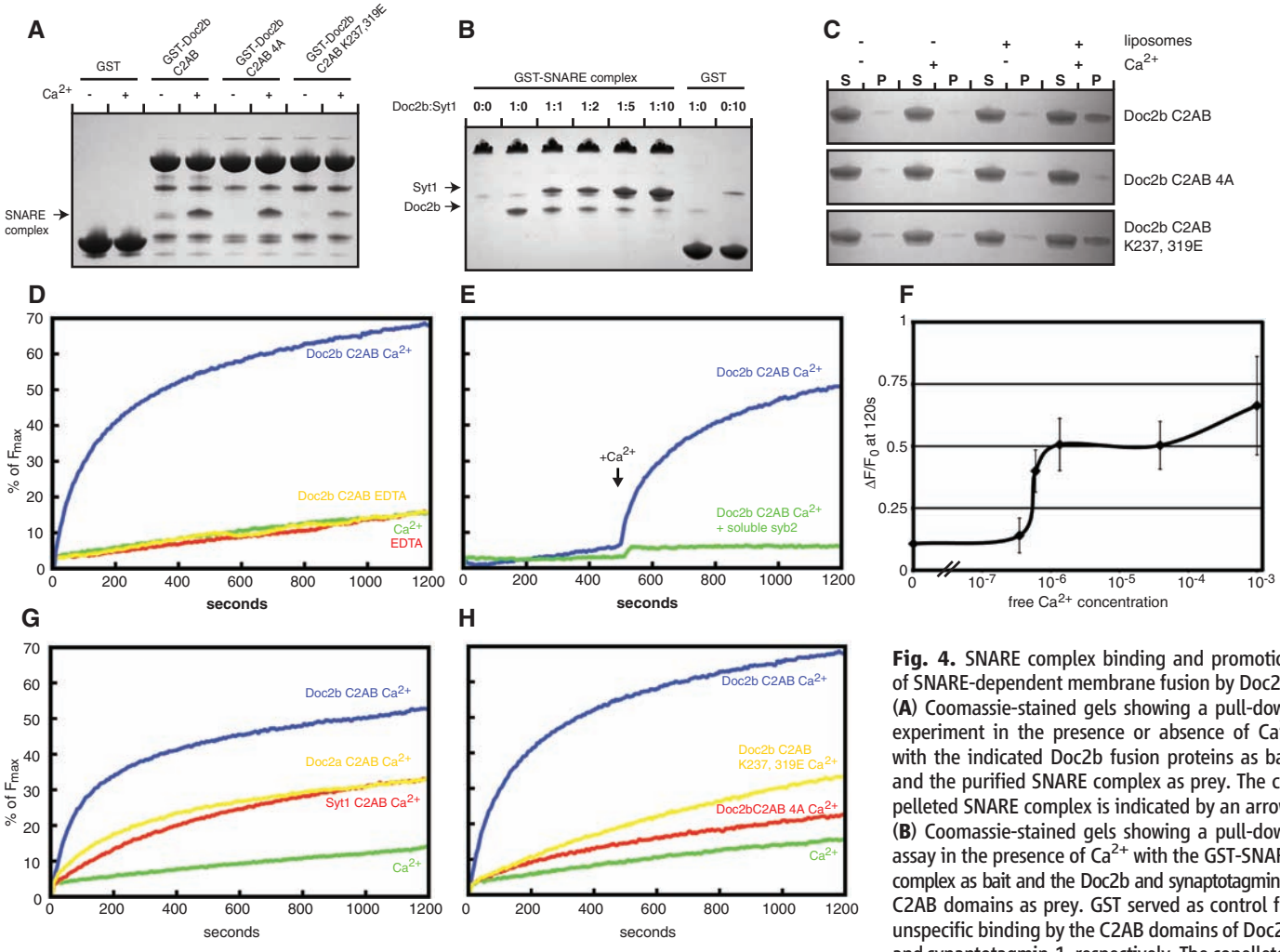

Fig. 4. SNARE complex binding and promotion of SNARE-dependent membrane fusion by Doc2b. (**A**) Coomassie-stained gels showing a pull-down experiment in the presence or absence of Ca^{2+} with the indicated Doc2b fusion proteins as bait and the purified SNARE complex as prey. The co-pelleted SNARE complex is indicated by an arrow. (**B**) Coomassie-stained gels showing a pull-down assay in the presence of Ca^{2+} with the GST-SNARE complex as bait and the Doc2b and synaptotagmin-1 C2AB domains as prey. GST served as control for unspecific binding by the C2AB domains of Doc2B and synaptotagmin-1, respectively. The copelleted Doc2B and synaptotagmin-1 C2AB domains are indicated by arrows. (**C**) Liposome cosedimentation assay in the presence or absence of Ca^{2+} with the indicated proteins and liposomes composed of 20% PS, 70% PC, and 10% cholesterol. (**D**) In vitro membrane fusion assay with reconstituted full-length SNAREs in the absence or presence of Ca^{2+} and/or 7.5 μM Doc2b C2AB. (**E**) In vitro membrane fusion assay as in (D) but in the presence or absence of the soluble SNARE domain of synaptobrevin. Ca^{2+} was added at 500 s. (**F**) Ca^{2+} dose-dependence curve showing the change of fluorescence at 120 s in the reconstituted fusion assay in the presence of 7.5 μM Doc2b. Doc2b efficiently promotes fusion at submicromolar Ca^{2+} concentrations. The graph summarizes data from three independent experiments. (**G**) Comparison of the fusion-promoting activities of the Doc2b, Doc2a, and synaptotagmin-1 C2AB domains. (**H**) Fusion experiment using the indicated Doc2b C2AB proteins reveals that Ca^{2+}-dependent membrane and SNARE-binding are required for efficient fusion promotion. All data shown are representative of at least three independent experiments.

formed at postnatal day P17 in the absence of DNQX or TTX. We observed various firing patterns in PCs from wild-type or heterozygous mice: irregular trains of simple spikes in most cells (Fig. 2D) or trimodal firing patterns composed of tonic, burst, and silent periods, as expected (*31*, *32*). In contrast, PCs from *Doc2b*$^{-/-}$ mice showed continuous spiking without interruptions (Fig. 2E). This pattern occurred with a frequency of 20 to 25 Hz and was observed in all *Doc2b*$^{-/-}$ cells tested, but never in control cells.

We also investigated neurotransmission in the calyx of Held synapse, a giant glutamatergic synapse in the auditory brainstem where the Doc2-Munc13 interaction is suggested to contribute to presynaptic plasticity (*33*). DKO mice exhibited normal evoked responses with a lower spontaneous release frequency by a factor of two (1.9 Hz compared with 4.8 Hz in control littermates), but this difference did not reach statistical significance (fig. S4).

Phospholipid and SNARE interactions. Doc2b is structurally similar to synaptotagmin-1 but lacks a transmembrane domain, and its C2 domains have a relatively high Ca^{2+} affinity (*26*). It is thus conceivable that Doc2b mediates spontaneous release events similar to synaptotagmin-dependent synchronous release, only with slower kinetics and a higher Ca^{2+} sensitivity. We thus tested if Doc2b is biochemically similar to synaptotagmin-1.

The Doc2b C2A domain bound in a Ca^{2+}-dependent manner to phosphatidylserine-containing membranes (Fig. 3A) (*34*, *35*). In addition, the C2B domain showed weak Ca^{2+}-dependent phospholipid binding (Fig. 3A). The C2AB fragment of Doc2b showed stronger liposome binding than the isolated C2A and C2B domains (Fig. 3A). Ca^{2+}-dependent membrane binding by synaptotagmin-1 was enhanced in the presence of phosphatidylinositol 4,5-bisphosphate (PIP_2) (*36*). For the C2A and C2B domains of Doc2b, the inclusion of PIP_2 enhanced both Ca^{2+}-dependent and Ca^{2+}-independent binding (Fig. 3B). This Ca^{2+}-independent binding was localized to two polybasic patches on the C2A and C2B domains, respectively (figs. S5 and S6). The use of brain-derived Folch lipids (*37*) generally increased binding, including the Ca^{2+}-independent binding by the C2A domain (Fig. 3C and fig. S6). The C2AB domains of Doc2a and synaptotagmin-1 displayed similar behavior (Fig. 3D).

The C2AB domains of synaptotagmin-1, -3, and -5 induce a high degree of positive membrane curvature in a Ca^{2+}-dependent manner (*3*), owing to the insertion of the tips of both C2 domains into the hydrophobic phase of the membrane. Shallow insertions into a monolayer are known to induce bending of the membrane toward the insertion (*38*–*40*). In order to examine if Doc2b also induces membrane curvature, we incubated liposomes derived from Folch lipids with 10 μM Doc2b C2AB domain in the absence (EDTA only) or presence of Ca^{2+} (Fig. 3E). Indeed, the Doc2b C2AB domain efficiently induced tubulation of otherwise spherical liposomes in a strictly Ca^{2+}-dependent manner (Fig. 3E). We frequently observed closely aligned tubules, which indicated that the Doc2b C2AB domain could cluster liposomes in addition to their tubulation. Tubulation was still apparent at a Doc2b concentration of 5 μM but was barely detectable below 1 μM.

Synaptotagmin-1 requires SNARE complex binding to promote fusion in vitro and in vivo (*4*, *5*). We thus tested if Doc2b also bound SNARE complexes. In one set of experiments we assembled the SNARE core complex on glutathione beads with the synaptobrevin SNARE domain fused to glutathione *S*-transferase (GST) (fig. S7). The Doc2b and synaptotagmin-1 C2AB domains were subsequently added in the presence or absence of Ca^{2+}. In another set of experiments we used the GST-Doc2b C2AB domain to pull down the soluble SNARE complex (Fig. 4A). As expected (*41*), we found efficient Ca^{2+}-dependent binding of the synaptotagmin-1 C2AB domain to SNARE complexes (fig. S7). The Doc2b C2AB domain also bound to SNARE complexes (Fig. 4A and fig. S7). In the C2B domain of synaptotagmin-1, the same poly-lysine motif that binds PIP_2 mediates SNARE complex binding (*36*). We thus tested SNARE complex binding by the mutant C2AB^{K237,319E} domain of Doc2b (*42*). As expected, it showed a profound loss of SNARE complex binding (Fig. 4A and fig. S7). Next, we tested if the putative membrane inserting hydrophobic amino acids in the tips of the Ca^{2+} binding loops (Fig. 4A and fig. S7) contributed to SNARE complex binding. To this end we mutated H158, F222, and I360A. The first Ca^{2+} binding loop of the Doc2b C2B domain contains an alanine and so was not mutated. We refer to this mutant as the 4A mutant. It showed no defect in SNARE complex binding, which indicated that, as for synaptotagmin-1, SNARE complex and membrane binding can occur at the same time (Fig. 4A and fig. S7). In contrast, Ca^{2+}-dependent liposome binding was affected by only the 4A but not the K237,319E mutation (Fig. 4C). The decreased binding of the 4A mutant was less pronounced if the liposomes were made with higher percentages of phosphatidylserine.

The high structural and biochemical similarities between Doc2b and synaptotagmin-1 suggest that the binding site on the SNARE complex may be identical. We therefore tested if the C2AB domain of synaptotagmin-1 competes with the C2AB domain of Doc2b for SNARE complex binding (Fig. 4B). Indeed, increasing amounts of the synaptotagmin-1 C2AB domain competed away the Doc2b C2AB domain, which suggested that the binding sites for synaptotagmin-1 and DOC2B are overlapping.

Ca^{2+}-dependent promotion of membrane fusion by Doc2b. The C2AB domains of several members of the synaptotagmin family promote fusion of liposomes containing reconstituted SNAREs in a Ca^{2+}-dependent manner (*43*). Similarly, the C2AB domain of Doc2b promoted fusion of SNARE-containing liposomes, and this activity was strictly Ca^{2+} dependent (Fig. 4, D to H). When Ca^{2+} was introduced at a later time, the fusion-promoting effect was even more apparent (Fig. 4E). The fusion-promoting activity of Doc2b was SNARE dependent (Fig. 4E). If Doc2b acts as a Ca^{2+} sensor for spontaneous synaptic vesicle fusion, it is likely to be activated by intracellular Ca^{2+} in the submicromolar range (*26*). Consistent with this, Doc2b bound to membranes with a submicromolar affinity (fig. S8), and at submicromolar Ca^{2+}, Doc2b promoted fusion (Fig. 4F). The in vitro fusion-promoting effect of Doc2b far exceeded that of synaptotagmin-1 and Doc2a (Fig. 4G). Next, we tested if Ca^{2+}-dependent mem-

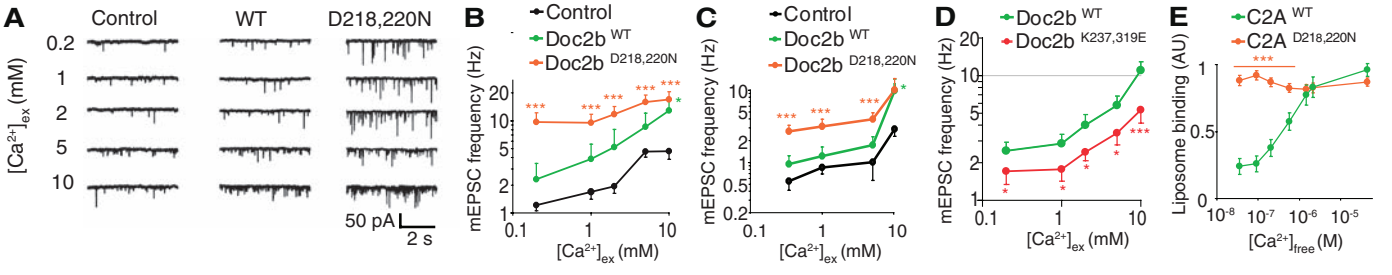

Fig. 5. The Ca^{2+} dependence of Doc2b determines that of spontaneous release in rescued DKO neurons. (**A**) Typical mEPSC recordings in DKO cells rescued with GFP (control), Doc2b^{WT}, or Doc2b^{D218,220N}. Spontaneous mEPSCs were recorded in network cultures of hippocampal neurons in the presence of TTX and gabazine. Increasing concentrations of extracellular Ca^{2+} were administered to the same cell. (**B**) Mean mEPSC frequencies ± sem in DKO cells expressing Doc2b^{WT} ($n = 10$), Doc2b^{D218,220N} ($n = 26$) or GFP as a control ($n = 21$). (**C**) Mean mEPSC frequencies of the same constructs expressed in wild-type cells. The average mEPSC frequency varied between experiments, but our experimental design prevents confounding effects thereof (see fig. S2E). (**D**) Mean mEPSC frequencies in DKO cells expressing Doc2b^{WT} ($n = 35$) or mutant Doc2b^{K237,319E} ($n = 31$). (**E**) Ca^{2+}-dependent liposome-binding by the isolated C2A domain of Doc2b^{WT} and Doc2b^{D218,220N} ($n = 6$). ***$P < 0.005$; **$P < 0.01$, *$P < 0.05$.

brane binding and SNARE binding were required for the strong fusion-promoting effect of Doc2b. Indeed, both mutant Doc2b^{4A} impaired in Ca^{2+}-dependent phospholipid binding (fig. S8) and mutant Doc2b^{K237,319E} impaired in SNARE binding (Fig. 4A) promoted fusion to a lesser extent than wild-type Doc2b (Fig. 4H).

Ca^{2+} dependence of Doc2b-driven spontaneous release. If Doc2b generates spontaneous events by acting as a Ca^{2+} sensor, then mutagenesis of its Ca^{2+} binding site should affect the Ca^{2+} dependence of spontaneous release. We thus expressed wild-type or mutant Doc2b in DKO neurons in network cultures (*10*, *11*). The Ca^{2+} dependence of spontaneous release was assessed by superfusing neurons with increasing extracellular Ca^{2+} concentrations (from 0.2 to 10 mM) (Fig. 5A). As expected, the spontaneous release rate increased with increasing Ca^{2+} concentrations (Fig. 5B) (*11*). Mutant Doc2b^{D218,220N}, which mimics a dominant active Ca^{2+}-bound state of the C2A domain (*19*), caused a massive increase in spontaneous release rate, especially at low Ca^{2+} concentrations (Fig. 5, B and C). The Ca^{2+} dependence of spontaneous release was almost completely lost in Doc2b^{D218,220N}-expressing cells. This correlated well with the Ca^{2+}-independent binding of the isolated C2A^{D218,220N} or C2AB^{D218,220N} fragment to liposomes (Fig. 5E and fig. S8). DKO neurons expressing wild-type Doc2b had a higher spontaneous release rate at each Ca^{2+} concentration than DKO neurons expressing GFP (Fig. 5B). Even in cells lacking Doc2, we observed more spontaneous release events at higher Ca^{2+} concentrations, albeit less pronounced than in wild-type or rescued cells. Thus, as seen before (Fig. 1), additional high-affinity Ca^{2+} sensors for spontaneous release may exist. At high extracellular Ca^{2+} concentrations (5 to 10 mM), the spontaneous release rate increased in all groups, a release that may be supported by synaptotagmins (*11*). We also expressed Doc2b^{WT} and Doc2b^{D218,220N} in neurons from wild-type mice. Consistent with the data from DKO neurons, expression of each construct increased the spontaneous release rate. This was most pronounced in Doc2b^{D218,220N}-expressing cells (Fig. 5C). Conversely, overexpression of a loss-of-function mutant, Doc2b^{K237,319E}, caused significantly lower mEPSC frequencies at all Ca^{2+} concentrations compared with Doc2b^{WT} in DKO neurons (Fig. 5D). Because PIP_2 binds to the same region as SNAREs (*36*), we cannot exclude a contribution of PIP_2 binding in this experiment. However, our in vitro fusion assay was performed in the absence of PIP_2 so here, the profound loss of Doc2b^{K237,319E} function was almost certainly due to its loss of Ca^{2+}-dependent SNARE-binding (Fig. 4H). Thus, manipulation of the Ca^{2+} dependence of Doc2b affected the Ca^{2+} dependence of spontaneous release, which implicates Doc2b as a Ca^{2+} sensor.

Conclusions. Here we have found that Doc2b is a high-affinity Ca^{2+} sensor for half (hippocampus) or most (cerebellum) of the spontaneous neurotransmitter release events in CNS synapses. Doc2b acts as a functional synaptotagmin-1 analog, operating at smaller Ca^{2+} increases and with higher in vitro fusion efficiency. In contrast to synaptotagmin-1, which has the appropriate affinity to respond to high Ca^{2+} peaks occurring at release sites, Doc2b requires less than 1 μM Ca^{2+} to enhance fusion. Doc2b is not associated with the synaptic vesicle via a transmembrane domain like synaptotagmins and translocates to membranes in response to Ca^{2+} (*34*), a quality that would explain why evoked release was unaffected in our study. Nevertheless, it is likely that Doc2 proteins are located not far from release sites because of its interactions with SNARE complexes (Fig. 4A), Munc13 (*20*, *44*), and Munc18 (*18*). Given the sensitivity of Doc2-dependent spontaneous release to BAPTA chelation (Fig. 1E), the protein must be activated close to a source of Ca^{2+}, whether this is a Ca^{2+} channel or an intracellular Ca^{2+} store (*12*–*15*).

Spontaneous release events appear to be mechanistically heterogeneous. In the synapses studied here, most spontaneous events are Ca^{2+} dependent and require Doc2. Because the spontaneous release in the absence of Doc2 remained sensitive to BAPTA and prolonged neuronal firing at 5 Hz, one or more additional high-affinity Ca^{2+} sensors probably exist. Finally, BAPTA did not block all spontaneous release events and thus, some events are probably truly Ca^{2+} independent, which may be supported by factors such as synaptotagmin-12 (*16*).

Because multiple C2 domain–containing proteins are coexpressed in synapses and at least Doc2b and synaptotagmin-1 compete for SNARE complex binding, a certain degree of redundancy probably exists among these protein families. The concentrations of various C2-domain proteins and their Ca^{2+} affinity will determine the Ca^{2+} sensitivity of release and the release probability of vesicles. Differences in this balance may explain the large differences in spontaneous release frequencies observed among neurons. Along the same lines, it is conceivable that the increased frequency of spontaneous release in synaptotagmin-1–deficient mice is triggered by Doc2 or other C2 domain–containing proteins (*41*, *45*, *46*) that replace synaptotagmin-1 in its absence, where, effectively, synaptotagmin would appear to clamp fusion (*11*). Finally, whereas spontaneous vesicle fusion could conceivably have been dependent on SNARE assembly alone, we now show that many of these events require the action of curvature-inducing multiple C2 domain proteins.

References and Notes

1. M. Geppert *et al.*, *Cell* **79**, 717 (1994).
2. R. Fernández-Chacón *et al.*, *Nature* **410**, 41 (2001).
3. S. Martens, M. M. Kozlov, H. T. McMahon, *Science* **316**, 1205 (2007).
4. K. L. Lynch *et al.*, *Mol. Biol. Cell* **19**, 5093 (2008).
5. Z. P. Pang, O. H. Shin, A. C. Meyer, C. Rosenmund, T. C. Südhof, *J. Neurosci.* **26**, 12556 (2006).
6. J. T. Littleton, M. Stern, K. Schulze, M. Perin, H. J. Bellen, *Cell* **74**, 1125 (1993).
7. A. DiAntonio, T. L. Schwarz, *Neuron* **12**, 909 (1994).
8. J. Sun *et al.*, *Nature* **450**, 676 (2007).
9. J. Xu, T. Mashimo, T. C. Südhof, *Neuron* **54**, 567 (2007).
10. H. Liu, C. Dean, C. P. Arthur, M. Dong, E. R. Chapman, *J. Neurosci.* **29**, 7395 (2009).
11. J. Xu, Z. P. Pang, O. H. Shin, T. C. Südhof, *Nat. Neurosci.* **12**, 759 (2009).
12. T. Collin, A. Marty, I. Llano, *Curr. Opin. Neurobiol.* **15**, 275 (2005).
13. N. J. Emptage, C. A. Reid, A. Fine, *Neuron* **29**, 197 (2001).
14. I. Llano *et al.*, *Nat. Neurosci.* **3**, 1256 (2000).
15. V. De Crescenzo *et al.*, *J. Neurosci.* **24**, 1226 (2004).
16. A. Maximov, O. H. Shin, X. Liu, T. C. Südhof, *J. Cell Biol.* **176**, 113 (2007).
17. S. Orita *et al.*, *Biochem. Biophys. Res. Commun.* **206**, 439 (1995).
18. M. Verhage *et al.*, *Neuron* **18**, 453 (1997).
19. R. Friedrich *et al.*, *J. Neurosci.* **28**, 6794 (2008).
20. S. Orita *et al.*, *J. Biol. Chem.* **272**, 16081 (1997).
21. B. Ke, E. Oh, D. C. Thurmond, *J. Biol. Chem.* **282**, 21786 (2007).
22. M. Miyazaki *et al.*, *Biochem. Biophys. Res. Commun.* **384**, 461 (2009).
23. N. Fukuda *et al.*, *Diabetes* **58**, 377 (2009).
24. Materials and methods are available as supporting material on Science Online.
25. Y. Otsu *et al.*, *J. Neurosci.* **24**, 420 (2004).
26. A. J. Groffen, R. Friedrich, E. C. Brian, U. Ashery, M. Verhage, *J. Neurochem.* **97**, 818 (2006).
27. J. E. Zengel, M. A. Sosa, *J. Physiol.* **477**, 267 (1994).
28. N. Korogod, X. Lou, R. Schneggenburger, *J. Neurosci.* **25**, 5127 (2005).
29. V. Chan-Palay, *Z. Anat. Entwicklungsgesch.* **134**, 200 (1971).
30. C. Bernard, H. Axelrad, *Brain Res.* **626**, 234 (1993).
31. B. E. McKay, R. W. Turner, *J. Physiol.* **567**, 829 (2005).
32. M. Womack, K. Khodakhah, *J. Neurosci.* **22**, 10603 (2002).
33. T. Hori, Y. Takai, T. Takahashi, *J. Neurosci.* **19**, 7262 (1999).
34. A. J. Groffen *et al.*, *J. Biol. Chem.* **279**, 23740 (2004).
35. T. Kojima, M. Fukuda, J. Aruga, K. Mikoshiba, *J. Biochem.* **120**, 671 (1996).
36. J. Bai, W. C. Tucker, E. R. Chapman, *Nat. Struct. Mol. Biol.* **11**, 36 (2004).
37. J. Folch, M. Lees, G. H. Sloane Stanley, *J. Biol. Chem.* **226**, 497 (1957).
38. F. Campelo, H. T. McMahon, M. M. Kozlov, *Biophys. J.* **95**, 2325 (2008).
39. M. G. Ford *et al.*, *Nature* **419**, 361 (2002).
40. S. Martens, H. T. McMahon, *Nat. Rev. Mol. Cell Biol.* **9**, 543 (2008).
41. J. Tang *et al.*, *Cell* **126**, 1175 (2006).
42. Single-letter abbreviations for the amino acid residues are as follows: A, Ala; C, Cys; D, Asp; E, Glu; F, Phe; G, Gly; H, His; I, Ile; K, Lys; L, Leu; M, Met; N, Asn; P, Pro; Q, Gln; R, Arg; S, Ser; T, Thr; V, Val; W, Trp; and Y, Tyr.
43. W. C. Tucker, T. Weber, E. R. Chapman, *Science* **304**, 435 (2004).
44. R. R. Duncan, A. Betz, M. J. Shipston, N. Brose, R. H. Chow, *J. Biol. Chem.* **274**, 27347 (1999).
45. Z. P. Pang, J. Sun, J. Rizo, A. Maximov, T. C. Südhof, *EMBO J.* **25**, 2039 (2006).
46. M. C. Chicka, E. Hui, H. Liu, E. R. Chapman, *Nat. Struct. Mol. Biol.* **15**, 827 (2008).

47. We thank R. Zalm, D. Schut, I. Saarloos, B. de Vries, C. van der Meer, and M. Schindler for technical assistance. H. Mansvelder and H. Lodder are acknowledged for expert advice and help in neurophysiology. This work was supported by the EU (EUSynapse project 019055 and Eurospin Health-F2-2009-241498 to M.V.), the U.K. Medical Research Council to H.M.M. and S.M., a European Molecular Biology Organization Long-Term Fellowship to S.M., and the Neuro-Bsik Mouse Phenomics Consortium BSIK03053 to M.V. The authors declare no conflicting interests.

Supporting Online Material

www.sciencemag.org/cgi/content/full/science.1183765/DC1
Materials and Methods
Figs. S1 to S8
Table S1
References

26 October 2009; accepted 1 February 2010
Published online 11 February 2010;
10.1126/science.1183765
Include this information when citing this paper.

www.sciencemag.org/cgi/content/full/science.1183765/DC1

Supporting Online Material for

Doc2b Is a High-Affinity Ca^{2+} Sensor for Spontaneous Neurotransmitter Release

Alexander J. Groffen,* Sascha Martens,* Rocío Díez Arazola, L. Niels Cornelisse, Natalia Lozovaya, Arthur P. H. de Jong, Natalia A. Goriounova, Ron L. P. Habets, Yoshimi Takai, J. Gerard Borst, Nils Brose, Harvey T. McMahon, Matthijs Verhage

*To whom correspondence should be addressed. E-mail: sander.groffen@cncr.vu.nl (A.J.G.) and sascha.martens@univie.ac.at (S.M.)

Published 11 February 2010 on *Science* Express
DOI: 10.1126/science.1183765

This PDF file includes

Supporting Online Material

Doc2b is a High Affinity Ca^{2+} Sensor for Spontaneous Neurotransmitter Release

Alexander J. Groffen[1,8,*], Sascha Martens[2,3,8,*], Rocío Díez Arazola[1], L. Niels Cornelisse[1], Natalia Lozovaya[1,4], Arthur P. H. de Jong[1], Natalia A. Goriounova[1,4], Ron L. P. Habets[5], Yoshimi Takai[6], J. Gerard Borst[5], Nils Brose[7], Harvey T. McMahon[2,8] and Matthijs Verhage[1,8]

MATERIALS AND METHODS

Antibodies

To cross-absorb a previously described antiserum pAb13.2 raised against amino acids 22-116 of rat Doc2b *(S1)*, a 2-ml column of cyanogen bromide-activated Sepharose beads conjugated to total brain lysate obtained from adult *Doc2a-b* double knockout mice. Fraction 5 of the flow through stained endogenous Doc2a and -b with no remaining signal of each protein in single and double-knockout mice. The dilution in phosphate-buffered saline was 1:100 or 1:500 for cytochemistry and blotting. Munc18-1 (pAb 2701, 1:2500) was home-made and validated against brain lysate from Munc18 null mice. Antibodies against synaptobrevin-2 (mAb 69.1, 1:2000 for cytochemistry or 1:5000 for blotting), munc13-1 (mAb 266B1, 1:1000), rab3 (mAb 42.1, 1:2000), α/β-SNAP (mAb 77.2, 1:2000), syntaxin-1 (mAb HPC-1, 1:5000) and α–tubulin (mAb 3A2, 1:5000) were from Synaptic Systems. Anti-SNAP25 (mAb SM181, 1:5000) was from Sternberger. Anti-MAP2 (chicken pAb ab5392, 1:20000) was from Abcam. Polyclonals against synaptotagmin-1 (pAb W855), -2 (I735), and -12 were a kind gift from Prof. T. Südhof and Dr. A. Maximov *(S2)*. Goat-anti-mouse-Alexa488, goat-anti-rabbit-Alexa546 and goat-anti-chicken-Alexa647 (all 1:1000) were from Invitrogen. Western blot signals were produced by enhanced chemifluorescence, digitized with the FLA-5000 imaging system and quantified with AIDA imager analyzer software (Raytest).

Generation of knock-out mice

Animals were housed and bred according to institutional, Dutch, and US governmental guidelines. To generate Doc2b knock-out mice, a 16 kb genomic fragment was obtained from a λZAP 129/SvJ mouse genomic library (Stratagene) and used to construct a gene replacement vector designed to replace the *Mlu*I-*Sal*I fragment with the *Doc2b* promoter and exon 1 by a floxed neomycin gene oriented in the antisense direction. The targeting vector was linearized with *Spe*I and electroporated into the mouse embryonic stem cell line E14.1, originating from the inbred strain 129P2/OlaHsd. Clones resistant to 450 μg/ml G418 (Invitrogen) were isolated and tested for homologous recombination by PCR amplification and Southern blotting. Correctly targeted ES cells were injected into blastocysts and implanted in pseudopregnant females. Chimeric males were mated to C57BL/6 inbred females and heterozygous F1 offspring was backcrossed for more than 10 generations to C57BL/6 to ensure a homogenous genetic background. To exclude expression of the remaining exons in the targeted allele, RT-PCR amplification was performed with primers mav221 (caatgatttcatcggtg) and mav204 (tgagaaagcccagggttg). Since the *Doc2b* null allele lacks exon 1, in situ hybridization was performed with a probe that hybridizes with exons 2-9 (nucleotides 512-1378 of the mRNA) as described previously *(S3)*. Doc2a/b double knock-out mice were obtained by breeding with previously established Doc2a null mice *(S4)*.

Autapse electrophysiology

To prepare autapses, neurons were dissociated from hippocampi at embryonal stage E18 and plated on glial microislands *(S5)*. Whole-cell recordings were performed at room temperature between 14 and 18 days in vitro. The intracellular solution was free of EGTA; it contained 125 mM K^+-gluconic acid, 10 mM NaCl, 4.6 mM $MgCl_2$, 4 mM K_2-ATP, 15 mM creatine phosphate, 10 U/ml phosphocreatine kinase (pH=7.30, 300 mOsmol). The external medium contained 140 mM NaCl, 2.4 mM KCl, 4 mM $CaCl_2$, 4 mM $MgCl_2$, 10 mM glucose and 10 mM HEPES (pH 7.30, 300 mOsmol). Clampfit v9.2 was used for offline analysis of evoked EPSCs. Miniature EPSCs were detected using Mini Analysis v6.0.3 (Synaptosoft Inc) using a threshold amplitude of 10 pA. To calculate synchronous and asynchronous components of the EPSC charge as described *(S6)*, a home-made routine was written in the MATLAB® environment (MathWorks).

For overexpression of full length rat Doc2b neurons were infected 8-15 h prior to analysis with Semliki particles encoding full length rat Doc2b and GFP, separated by an internal ribosome entry site. To control for effects caused by the Semliki infection we used particles encoding GFP alone. Recordings and analysis were performed while the identity of experimental groups was unknown to the experimenter. To monitor the expression and localization of overexpressed Doc2b, cells were fixed 12 h post infection with 4 % paraformaldehyde, stained as indicated above (see antibodies) and analyzed on a LSM510 confocal microscope (Zeiss).

To test the influence of EGTA and BAPTA on spontaneous release, spontaneous events were recorded first in naïve cells during 1 min, followed by a EPSC recording after stimulation. Cells were then incubated for 15 minutes in presence of 20 µM of AM-EGTA or AM-BAPTA (Invitrogen) in the bath solution. Successful BAPTA loading was confirmed by the inhibition of EPSC amplitude using 1 min stimulation intervals to avoid activity-induced artifacts.

mEPSC frequency in primary network cultures

Hippocampal neurons from Doc2a/b double knockout mice were prepared as previously described *(S7)* except that the neurons were plated at 50K per 12-well on a confluent layer of glia. The cells were infected with lentiviral vectors encoding GFP, $Doc2b^{WT}$, $Doc2b^{4A}$ or $Doc2b^{D218,220N}$ on DIV2. The infection efficiency was >90% for all constructs as confirmed by immunocytochemistry. For whole-cell recordings at DIV10-17 the neurons were analyzed with the same internal and external media as in autapses, except that the bath contained 1 mM Mg^{2+}, 1 µM tetrodotoxin to block Na+ currents (Ascent) and 20 µM gabazine to block $GABA_A$ receptor mediated currents (Sigma). The Ca^{2+} concentration was varied from 0.2 to 1, 2, 5, 10 and then back to 0.2 mM by superfusion. mEPSC frequencies were quantitated as above; cells that never reached frequencies >0.2 Hz even at 10 mM Ca^{2+} or with frequencies >12 Hz in 0.2 mM Ca^{2+} were excluded from analysis (3 cells of 73 in total). The mEPSC frequency during the first and second measurement in 0.2 mM Ca^{2+} did not deviate substantially, suggesting that the treatment did not compromise cell viability. The experimenters were blind to the expressed constructs during the recordings and analysis.

Whole-cell recordings in cerebellar Purkinje cells

Spontaneous GABAergic input to Purkinje cells was measured in acute slices *(S8)*. The extracellular medium contained 125 mM NaCl, 3 mM KCl, 1.2 mM NaH2PO4, 26 mM NaHCO3, 10 mM glucose, 1 mM Mg2+ and 2 mM Ca^{2+}. Spontaneous events were recorded in presence of tetrodotoxin and DNQX to block AMPA receptors. To verify that these conditions effectively blocked Purkinje cell firing, we confirmed that Ca^{2+}-spikes and NMDA currents were absent. The intracellular solution contained 141 mM CsCl, 2 mM MgATP, 10

mM tetraethyl ammonium and 10 mM HEPES (pH 7.3) for voltage clamp recordings at age P6-P7, or 130 mM K-gluconate, 10 mM Na-gluconate, 4 mM NaCl, 4 mM MgATP, 0.3 mM NaGTP, 4 mM phosphocreatine and 10 mM HEPES (pH 7.3) for current clamp recordings at age P17-P18. Recordings and analysis were performed while the identity of experimental groups was unknown to the experimenter.

Calyx of Held electrophysiology

Acute slices were prepared as described *(S9)*. In brief, 8- to 10-day old pups were obtained from a mating between *Doc2a*$^{+/-}$, *Doc2b*$^{+/-}$ and *Doc2a*$^{-/-}$, *Doc2b*$^{-/-}$ mice. The number of mice investigated was: control (*Doc2a*$^{+/-}$ and *Doc2b*$^{+/-}$; N=4), Doc2a-deficient (*Doc2a*$^{-/-}$ and *Doc2b*$^{+/-}$; N=5), *Doc2b*-deficient (*Doc2a*$^{+/-}$ and *Doc2b*$^{-/-}$; N=3), and DKO (*Doc2a*$^{-/-}$ and *Doc2b*$^{-/-}$; N=6).#Principal cells in the medial nucleus of the trapezoid body were selected for postsynaptic action potential firing upon stimulation of the axons originating from the cochlear nucleus. Whole-cell voltage clamp recordings were made with an Axopatch 200B amplifier (Molecular Devices, Union City, CA, USA) at a holding potential of –80 mV. Potentials were corrected for a –11 mV junction potential. Series resistance did not exceed 15 MOhm and was compensated for at least 90%. Signals were low-pass filtered at 2 kHz and digitized at 20–50 kHz with a Digidata 1320A (Molecular Devices). Miniature EPSCs were detected in Clampfit 9 with a template based search method (match threshold = 4). This threshold defines how well the mEPSC should match the rise time and decay time of a predefined template. In some experiments kynurenic acid (2mM, Tocris, Bristol, UK) was washed in to prevent post-synaptic receptor saturation and desensitization. Recovery from depression was measured with two 100 Hz trains with known interval (in kynurenic acid). All recordings and analysis were performed blind to the post-hoc determined genotype.

Statistical analyses

Because the spontaneous release frequency is not normally distributed as indicated by a D'Agostino-Pearson normality test ($p<0.0001$), we applied the nonparametric Mann-Whitney test for independent samples. The spontaneous release frequencies before and after loading of a Ca^{2+} chelator in the same cell were compared by a Wilcoxon rank sum test for paired samples. All P-values represent two-tailed probabilities.

Protein expression and purification

All synaptotagmin-1, Doc2a and Doc2b fragments were expressed as glutathione-S-transferase (GST) fusion proteins from pGEX4T2 or pGEX4T1. The C2AB domain constructs comprised amino acids 96-421 of rat synaptotagmin-1 (NP_001028852), amino acids 88-400 of rat Doc2a (NP_075226) and amino acids 125-412 of rat Doc2b (NP_112404). The C2A domain comprised amino acids 125-255 of rat Doc2b and the C2B domain comprised amino acids 265-412 of rat Doc2b. Mutations were introduced according to the Stratagene QuikChange protocol.

BL21(DE3) pLysS cells (Stratagene) were used for expression of the synaptotagmin-1, Doc2a and Doc2b C2A, C2B and C2AB domain fragments. Cells were grown at 37°C until 0.3 OD_{600}, induced with 40 µM Isopropyl β-thiogalactopyranoside (IPTG) and grown for 14-16 h at 18°C. Cells were harvested and resuspended in 50 mM HEPES pH 7.5, 300 mM NaCl, 4 mM dithiothreitol (DTT), 2 mM $MgCl_2$, DNaseI, RNaseA and lysed by freeze thawing. The lysate was centrifuged for 45 min at 125,000 g, 4°C and the supernatant was incubated with 1 ml of glutathione beads (GE healthcare) per 1 l of culture for 1-2 h. Beads were washed 7 times with 50 mM HEPES pH 7.5, 300 mM NaCl, 4 mM DTT followed by two 15 min washes with 50 mM HEPES pH 7.5, 700 mM NaCl, 4 mM DTT, 2 mM $MgCl_2$, DNaseI, RNaseA. The protein was cleaved off the beads with thrombin by over night incubation at

16°C. The supernatant was concentrated and the protein was further purified by gelfiltration in 50 mM HEPES pH 7.5, 150 mM NaCl, 4 mM DTT using a HiLoad 16/60 Superdex 75 column (Pharamcia Biotech). For pull downs the GST-fusion proteins were purified as described above except that the protein was eluted from the glutathione beads with 20 mM glutathione and subsequently purified by gelfiltration in 50 mM HEPES pH 7.5, 150 mM NaCl, 4 mM DTT using a HiLoad 16/60 Superdex 200 column (Pharamcia Biotech). The proteins were shock frozen and stored at -80°C. Possible protein and RNA contamination was checked by SDS gel electrophoresis and UV spectroscopy, respectively.

Rat full length SNAP-25 (NP_112253) and full length syntaxin-1 (NP_446240) were expressed as GST fusion proteins in BL21(DE3) pLysS cells (Stratagene). Cells were grown at 37°C until OD_{600} of 0.9-1, induced with 500 µM IPTG and grown for 4 h at 37°C. Cells were harvested and resuspended in 50 mM Tris pH 8, 300 mM KCl, 10% glycerol, 5% Triton X-100, 5 mM DTT, 2 mM $MgCl_2$, DNaseI, EDTA-free Complete protease inhibitors (Roche) and lysed by freeze thawing. The lysate was centrifuged for 45 min at 125,000g, 4°C and the supernatant was incubated with 1 ml of glutathione beads (GE Healthcare) per 1 l of culture for 1-2 h. Beads were washed 6x with 50 mM Tris pH 8, 300 mM KCl, 10% glycerol, 1% Triton X-100, 5 mM DTT, EDTA-free Complete protease inhibitors (Roche) and two 15 minute washes with 50 mM Tris pH 8, 700 mM KCl, 10% glycerol, 1% Triton X-100, 5 mM DTT. Subsequently the beads were washed with over 20 bead volumes of 50 mM Tris pH 8, 100 mM KCl, 10% glycerol 0.8% w/v n-octyl β-D-glucopyranoside (OGP), 5 mM DTT. SNAP-25 and syntaxin-1a were cleaved off the beads with thrombin over night at 16°C. Thrombin was then inactivated by the addition of 0.1 mM phenylmethylsulphonyl fluoride (PMSF) followed by 1 h incubation at room temperature. The supernatant was shock frozen and stored at -80°C. The functionality of SNAP25, syntaxin1 and synaptobrevin was monitored by SDS-resistant SNARE complex formation.

Rat full length synaptobrevin (NP_036795) was expressed as GST fusion protein from pGEX4T1 in BL21(DE3) pLysS cells. Cells were grown at 37°C until OD_{600} of 0.3, induced with 40 µM IPTG and grown for 14-16 h at 18°C. Cells were harvested and resuspended in 25 mM HEPES pH 7.5, 400 mM KCl, 1% Triton X-100, 2 mM $MgCl_2$, 4 mM DTT, EDTA-free Complete protease inhibitors (Roche), 0.2 mM PMSF, DNaseI. Cells were lysed by freeze thawing and the lysate was centrifuged for 45 min at 125,000g, 4°C and the supernatant was incubated with 1 ml of glutathione beads (GE healthcare) per 1 l of culture for 1-2 h. Beads were washed 6x with 25 mM HEPES pH 7.5, 400 mM KCl, 1% Triton X-100, 4 mM DTT, EDTA-free Complete protease inhibitors (Roche) and two 15 minutes washes with 25 mM HEPES pH 7.5, 700 mM KCl, 5% Triton X-100, 4 mM DTT. Subsequently with 25 mM HEPES pH7.5, 100 mM KCl, 10% glycerol, 1% w/v OGP, 4 mM DTT. Synaptobrevin was cleaved off the beads with thrombin over night at 4°C. Thrombin was then inactivated by the addition of 0.1 mM PMSF followed by 1 h incubation at room temperature. The supernatant was shock frozen and stored at -80°C.

The SNARE domains of rat synaptobrevin (amino acids 1-96), rat syntaxin1A (amino acids 180-265), rat SNAP25 (amino acids 11-82 and 141-206) were expressed as GST fusion proteins from pGEX4T1 in BL21(DE3) pLysS cells (Stratagene). Cells were grown at 37°C until OD_{600} of 0.3, induced with 40 µM IPTG and grown for 14-16 h at 18°C. Cells were harvested and resuspended in 50 mM HEPES pH 7.5, 300 mM NaCl, 4 mM DTT, 2 mM $MgCl_2$, DNaseI and lysed by freeze thawing. The lysate was centrifuged for 45 min at 125,000g, 4°C and the supernatant was incubated with 1 ml of glutathione beads (GE healthcare) per 1 l of culture for 1-2 h. Beads were washed 7 times with 50 mM HEPES pH 7.5, 300 mM NaCl, 4 mM DTT followed by two 15 min washes with 50 mM HEPES pH 7.5, 1 M NaCl, 1% Tx100 followed by 4 washes with 50 mM HEPES pH 7.5, 300 mM NaCl, 4 mM DTT. The protein was cleaved off the beads with thrombin by over night incubation at

4°C. The supernatant was concentrated and the protein was further purified by gelfiltration in 25 mM HEPES pH 7.5, 100 mM NaCl, 4 mM DTT using a HiLoad 16/60 Superdex 75 column (Pharamcia Biotech). For pull downs the GST-fusion proteins were purified as described above except that the protein was eluted from the glutathione beads with 20 mM glutathione and subsequently gelfiltered. The SNARE domains were then mixed in a ratio of 1:1:1:1 and incubated on room temperature for 2 h. The SNARE complex was further purified by gelfiltration in 25 mM HEPES pH 7.5, 100 mM NaCl, 4 mM DTT using a HiLoad 16/60 Superdex 75 column (Pharamcia Biotech) and finally concentrated, shock frozen and stored at -80°C.

For the co-expression of the synaptobrevin, SNAP25 and syntaxin1 SNARE domains the pOPC co-expression system was used. The synaptobrevin SNARE domain was first cloned into pOPTG to generate an N-terminal fusion protein. The SNARE domains of syntaxin1 and SNAP25 were cloned into pOPT. All SNARE domains were subsequently cloned into pOPC to generate the co-expression plasmid pOPC-SC. The pOPC-SC plasmid was transformed into BL21(DE3) pLysS cells (Stratagene) and the complex was purified as described for the isolated SNARE domains.

Possible protein and RNA contamination was checked by SDS gel electrophoresis and UV spectroscopy, respectively. The proteins are purified to crystallography standards.

Co-sedimentation assays

Liposomes were prepared using either Folch lipids (fraction1, Sigma) or 2.5% PtdIns(4,5)P_2 (Avanti #840046), 10% cholesterol (Sigma), 27.5% PtdSer (Avanti #840032), 60% PtdChol (Avanti #840053) or 10% cholesterol (Sigma), 25% PtdSer (Avanti #840032), 65% PtdChol (Avanti #840053). Lipids were combined, dried under argon, desiccated for 2h and buffer was added to a final concentration of 1mg/ml liposomes. 0.5 mg/ml liposomes were incubated with 20 µg of the proteins indicated in the figures. Ca^{2+} or EDTA (for the -Ca^{2+} samples) were added to a final concentration of 1 mM. After 30 min at room temperature the liposomes were centrifuged at 165,000g for 10 min at room temperature. Equal amounts of the supernatants and pellets were loaded on 4-12% gradient gels (Invitrogen). To determine the Ca^{2+} dose-dependence of phospholipid binding by the C2A domain, we used a previously described method *(S10)*.

Liposome tubulation assay by negative stain electron microscopy

Folch lipids (fraction 1, Sigma) were dried under argon, desiccated for 2 h and buffer was added to a final concentration of 1 mg/ml liposomes. 0.3 mg/ml Folch liposomes were incubated with 10 µM of the respective proteins in the presence of 1 mM EDTA or $CaCl_2$ for 1 h at room temperature and stained with 2% uranylacetate.

Pull down assays

For the pull down assay shown in Fig. 4A 30 µg of the GST- Doc2b C2AB domain was bound to 50 µl glutathione beads equilibrated in wash buffer (25 mM HEPES pH 7.5, 100 mM NaCl, 4 mM DTT). The proteins were bound to beads by a 30 min incubation at 4°C. The beads were washed 2 times with wash buffer plus 1 mM EDTA or $CaCl_2$, respectively. 30 µg of the purified SNARE complex was added followed by a 30 min incubation at 4°C. The beads were subsequently washed four times with wash buffer plus 1 mM EDTA or $CaCl_2$. Beads were resuspended in 60 µl SDS sample buffer, incubated for 10 min at room temperature, briefly centrifuged and 25 µl of the supernatant was loaded on a 4-12% gradient gel.

For the experiment shown in Fig. 4B 30µg of the co-expressed and purified GST-SNARE complex was bound to 20 µl glutathione beads for 1h at 4^0C. The beads were washed

and incubated with 17µg of Doc2b C2AB (1:0), 17µg of Doc2b C2AB and 17 µg of synaptotagmin-1 C2AB (1:1), 17µg of Doc2b C2AB and 34 µg of synaptotagmin-1 C2AB (1:2), 17µg of Doc2b C2AB and 85 µg of synaptotagmin-1 C2AB (1:5), 17µg of Doc2b C2AB and 170 µg of synaptotagmin-1 C2AB (1:10) in 50 mM HEPES pH 7.5, 100 mM NaCl, 4 mM DTT, 0.5 mM $CaCl_2$ for 1h at 4^0C. Incubation was followed by 2 washes with 50 mM HEPES pH 7.5, 100 mM NaCl, 4 mM DTT, 0.5 mM $CaCl_2$. Beads were resuspended in 50 µl SDS sample buffer, incubated for 10' at room temperature, briefly centrifuged and 10 µl of the supernatant was loaded on a 4-12% gradient gel.

For the pull down experiment shown in supplementary Fig. 7 30 µg of the GST-SNARE complex (assembled using individually purified SNARE domains) was bound to 50 µl glutathione beads equilibrated in wash buffer (25 mM HEPES pH 7.5, 100 mM NaCl, 4 mM DTT). The proteins were bound to beads by a 30 min incubation at 4°C. The beads were washed 2 times with wash buffer plus 1 mM EDTA or $CaCl_2$, respectively. 30 µg of the purified Doc2b C2AB domain and synaptotagmin-1 C2AB domain was added followed by a 30 min incubation at 4°C. The beads were subsequently washed four times with wash buffer plus 1 mM EDTA or $CaCl_2$. Beads were resuspended in 60 µl SDS sample buffer, incubated for 10 min at room temperature, briefly centrifuged and 25 µl of the supernatant was loaded on a 4-12% gradient gel.

Reconstitution of membrane fusion

The tSNARE and vSNARE liposomes were prepared by detergent assisted insertion into preformed liposomes as described previously *(S11)*.

tSNARE liposomes: To create a 20 mM liposome suspension lipids stored in chloroform were mixed in the following ratio: 25% phosphatidylserine (PtdSer) (Avanti #840032), 10% cholesterol (Sigma), 65% phosphatidylcholine (PtdChol) (Avanti #840053). Lipids were dried under argon and desiccated for 2 h. Lipids were re-hydrated by the addition of 50 mM Tris pH 8, 150 mM NaCl, 2 mM DTT. Lipids were incubated in the buffer for 15 min at room temperature and subsequently sonicated gently. The liposomes were then passed 9 times though an 800 nm filter (Whatman). 10 µl of the liposomes were then added to 90 µl of an 11.1µM tSNARE complex solution and incubated for 15 min at room temperature. The detergent was then diluted below the critical micelle concentration by the addition of 100 µl 50 mM Tris pH 8, 150 mM NaCl, 2 mM DTT. The liposomes were then dialyzed over night against 2 l of 25 mM HEPES pH 7.5, 100 mM KCl, 5% glycerol, 2 mM DTT, 10 g BioBeads (BioRad) at 4°C to remove the detergent and spun at 10,000g for 5 min at room temperature to remove aggregates. The supernatant was used for experiments.

vSNARE liposomes: To create a 10 mM liposome suspension lipids stored in chloroform were mixed in the following ratio: 15% phosphatidylserine (PtdSer) (Avanti #840032), 10% cholesterol (Sigma), 72% phosphatidylcholine (PtdChol) (Avanti #840053), 1.5% N-(7-nitro-2-1,3-benzoxadiazol-4-yl)-1,2-dipalmitoyl phosphatidylethanolamine (Invitrogen) and 1.5% rhodamine-phosphatidylethanolamine (Invitrogen), dried under argon and desiccated for 2 h. Lipids were rehydrated by the addition of 50 mM Tris pH 8, 150 mM NaCl, 2 mM DTT. Lipids were incubated in the buffer for 15 min at room temperature and sonicated gently. The liposomes were then passed 9 times though a 800 nm filter (Whatman). 20 µl of the liposomes were the added to 80 µl of a 50 µM solution of synaptobrevin and incubated for 15 min at room temperature. The detergent was then diluted below the critical micelle concentration by the addition of 100 µl 50 mM Tris pH 8, 150 mM NaCl, 2 mM DTT. The liposomes were then dialyzed over night against 2 l of 25 mM HEPES pH 7.5, 100 mM KCl, 5% glycerol, 2 mM DTT, 10 g BioBeads (BioRad) overnight at 4°C to remove the detergent and spun at 10,000g for 5 min at room temperature to remove aggregates. The supernatant was used for experiments.

Assuming a 100% efficient reconstitution of the proteins a protein/lipid ratio of 1:50 would be achieved for the vSNARE liposomes and a ratio of 1:100 for the tSNARE liposomes. As judged by co-flotation assays we achieved a reconstitution efficiency of about 90% for the vSNARE liposomes and 80% for the tSNARE liposomes. The integrity of the reconstituted proteo-liposomes was controlled by negative stain EM and the size distribution (60-70nm) was analyzed by dynamic light scattering. In addition the orientation of the SNAREs in the liposome membrane was analyzed by incubation with Botulinum neurotoxin E or Tetanus toxin. As expected for random integration only 50% of SNAP-25 and synaptobrevin, respectively were cleaved. The purity of the SNAREs used for the fusion experiments was over 90% as judged by SDS-PAGE and Coomassie staining.

For the fusion experiments 75 µl tSNARE liposomes were mixed with 25 µl vSNARE liposomes. The synaptotagmin-1, Doc2a and Doc2b fragments were added at a final concentration of 7.5 µM. The reactions were incubated on ice for 30 min before measurement. Ca^{2+} was added immediately before the measurement to final concentration of 500 µM. Fusion was monitored by dequenching of NBD upon dilution of the NBD incorporated in the vSNARE vesicles with the tSNARE vesicles after fusion. The NBD was excited at 465 nm and emission was detected at 530 nm. After 20 min 10% Triton X-100 was added to a final concentration of 1% to determine the maximum fluorescence. The Triton X-100 used in this study quenches the NBD fluorescence to about 70% of its maximum value. The increase of fluorescence mediated by SNARE/Doc2b/Ca^{2+} is thus lower by a factor of 1.4.

In order to facilitate detection of the initial fusion reaction we added a volume of 10 µl 5 mM $CaCl_2$ or EDTA in reaction buffer to the warm fusion reaction in the quartz cuvette. The measurement was started immediately after addition of 10 µl 5 mM $CaCl_2$ or EDTA (Fig. 4D, G, H) or after addition of 10 µl of EGTA buffered Ca^{2+}-solutions containing free Ca^{2+} concentrations of 0, 0.35, 0.6, 1.4, 39 and 1000 µM, respectively. (Fig. 4F). In the experiment shown in Fig. 4e $CaCl_2$ was added during the measurement.

In the experiment in which the soluble (amino acids 1-96) fragment of synaptobevin2 was added (Fig. 4E) the protein was added to a final concentration of 2 µM to pre-incubation reaction including v- and tSNARE liposomes and Doc2b C2AB.

Modelling of the Doc2b C2A and C2B domain structures

For the modelling of the Doc2b C2A and C2B domain structures Swissmodel was used (http://swissmodel.expasy.org). The rat Doc2b C2A domain sequence (amino acids 125-255) was submitted and modelled onto the structure of the rabphilin3a C2A domain crystal structure (PDB code 2chd) *(S12)*. The sequence identity between the Doc2b and rabphilin3A C2A domains is above 80%.

For the C2B domain the rat Doc2b C2B domain sequence (aa 265-412) was submitted and modelled onto the structure of the rabphilin3a C2B domain (PDB code 2cm5) *(S13)*. The sequence identity between the Doc2b and rabphilin3a C2B domains is 76%. The illustrations were created using CCP4 Molecular Graphics (available at http://www.ysbl.york.ac.uk/~ccp4mg/). The alignments were created with ClustalX 2.02 (ftp://ftp.ebi.ac.uk/pub/software/clustalw2) and manually modified using Genedoc (http://www.nrbsc.org/downloads/).

FIGURES AND TABLES

Figure S1

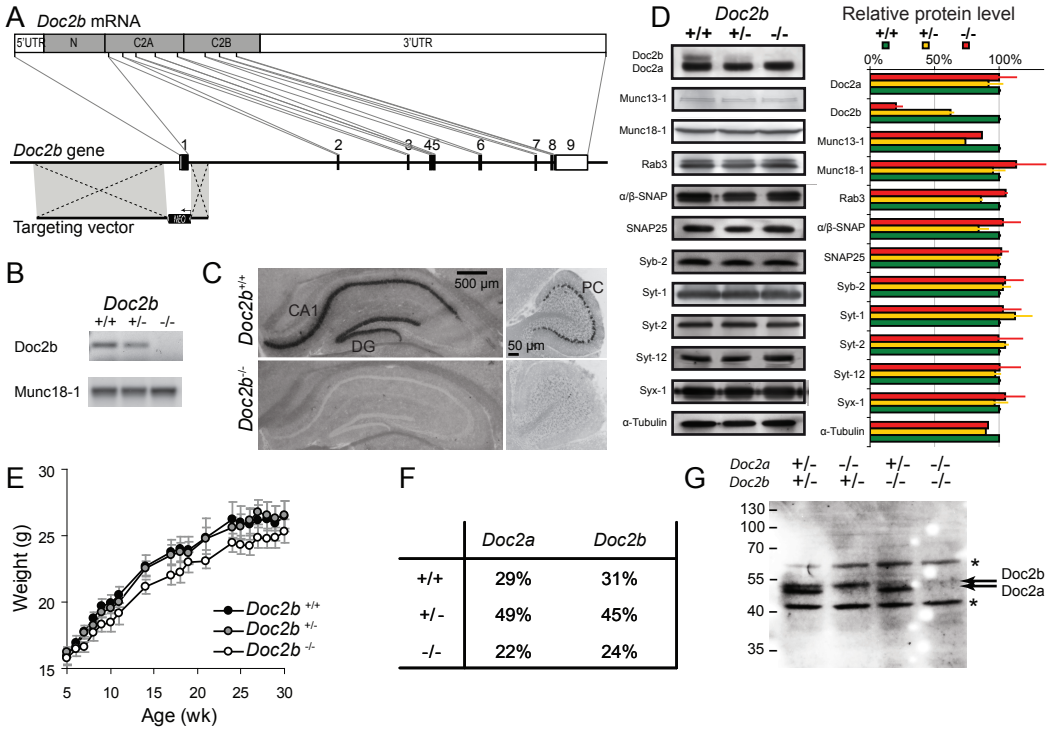

Fig. S1. Generation of *Doc2b* knock-out mice. (A) The promoter and exon 1 encoding the N-terminal domain of mouse Doc2b were deleted by homologous recombination. (B-C) No detectable expression of the remaining exons was detected by RT-PCR (B) or in situ hybridization (C) of adult *Doc2b*$^{-/-}$ mouse brains whereas Doc2b expression was prominent in the CA1 field and dentate gyrus (DG) of the hippocampus and the Purkinje cell (PC) layer of the cerebellum in wild-type littermates. (D) The loss of Doc2b immunoreactivity was not accompanied by changes in the immunoreactivity of other proteins tested in total brain lysate. The bar graph shows quantitation where we made repetitions: Doc2b (n=4); Doc2a (4); Munc13-1 (1); Munc18-1 (4); Rab3 (1); α/β-SNAP (3); SNAP25 (3); Synaptobrevin-2 (3); Synaptotagmin-1 (5); Synaptotagmin-2 (2); Synaptotagmin-12 (2); Syntaxin-1 (3); α-Tubulin (1). Note that the remaining Doc2b immunoreactivity reflects aspecific background signal. (E) *Doc2b*$^{-/-}$ mice were viable and fertile and developed a body weight that did not differ significantly from their wildtype littermates (N=13, 15 and 10 respectively for wildtypes, heterozygotes and homozygous null mice). (F) *Doc2b*$^{+/-}$ (N=409) and *Doc2a*$^{+/-}$ mice (N=225) yielded offspring with the expected Mendelian genotype frequencies. (G) Double-knockout mice were also viable and reached adulthood with no detectable Doc2a/b reactivity in adult brain lysate. The remaining bands represent cross-reactivity of the antibody with other gene products (asterisks).

Figure S2

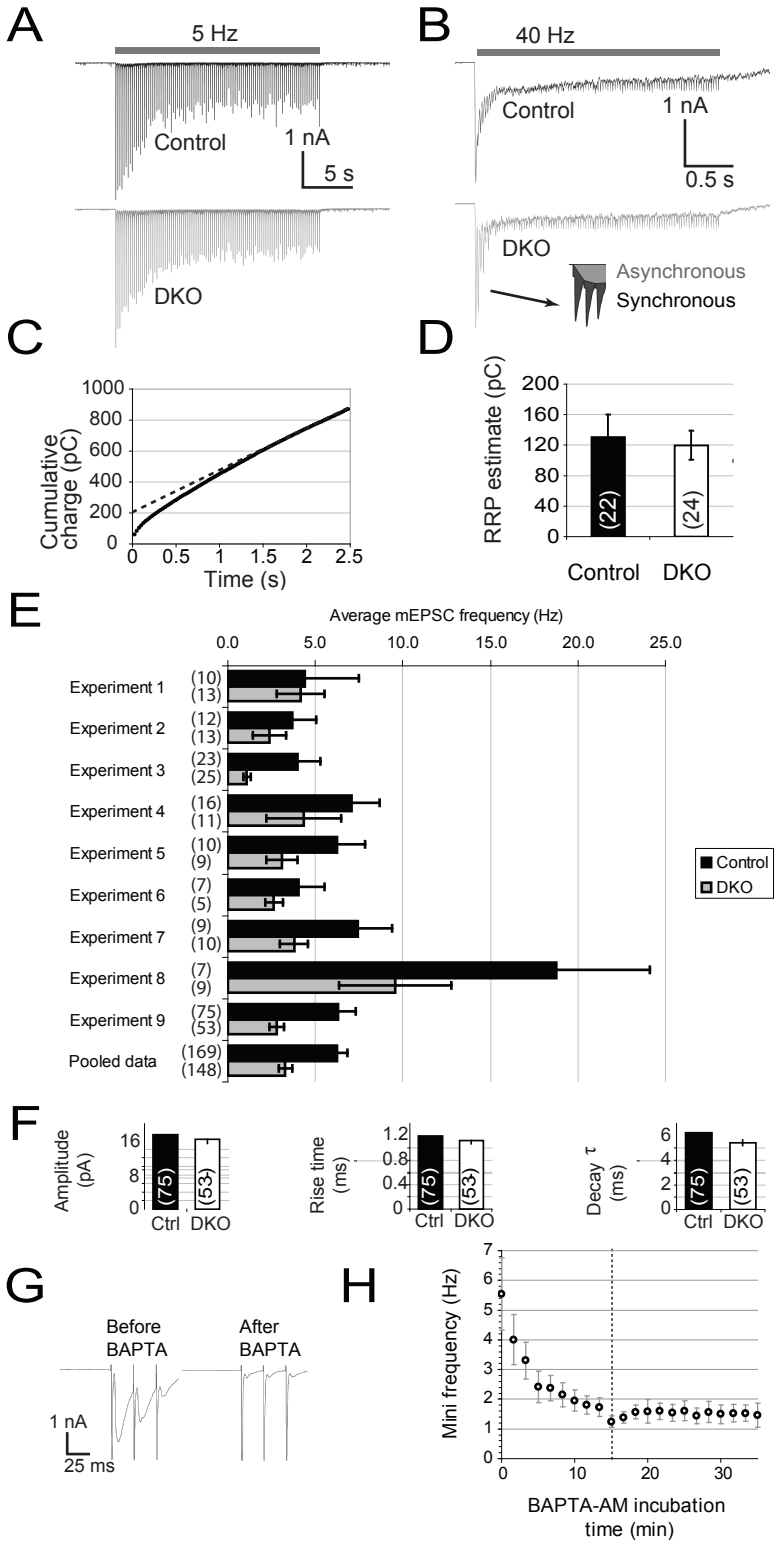

Fig. S2. Evoked and spontaneous release in hippocampal autapses from Doc2a/b-double knockout (DKO) mice. Data presented here are derived from the same experiments as Fig. 1. **(A, B)** Typical EPSC recordings during repetitive stimulation at 5 or 40 Hz. The synchronous and asynchronous components of the total charge were estimated as defined in the inset *(S6)*. **(C)** The RRP size was estimated by back-extrapolation of the cumulative charge during 40 Hz trains. Typical example is from a DKO cell. **(D)** Mean RRP size ± sem (number of observations is indicate between brackets). **(E)** Spontaneous release rates varied considerably between experiments. To exclude any confounding effects, we performed 9 different experiments in which simultaneously prepared cultures of WT and DKO cells were compared. Mean mEPSC frequencies ± sem are given with numbers of observations between brackets. 'Pooled data' corresponds to all observations taken together. **(F)** Postsynaptic parameters describing the shape and size of spontaneous release events in DKO and control cells. **(G)** In cells loaded with BAPTA, the ability of BAPTA to absorb Ca^{2+} transients was confirmed by an almost complete inhibition of evoked EPSCs. **(H)** Under the conditions used, the frequency of spontaneous release reaches a steady state after 15 min incubation with AM-BAPTA.

Figure S3

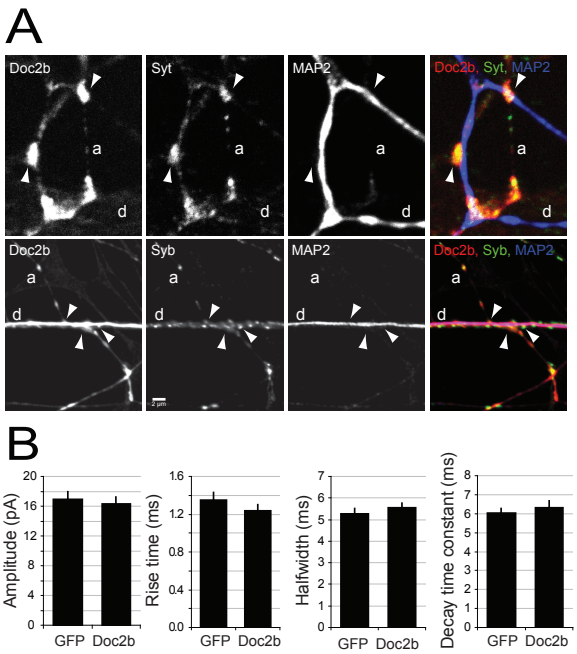

Fig. S3. Acute expression of Doc2b in DKO neurons. To test if acute overexpression of Doc2b affects spontaneous release, DKO neurons grown on glial microislands were infected with Semliki particles encoding Doc2b. **(A)** Immunoreactivity was observed in all subcellular compartments including the soma (not shown), dendrites (d), axons (a) and synapses (arrowheads). Cells were counterstained for MAP2 to mark dendrites and synaptotagmin (Syt) or synaptobrevin-2 (Syb) to mark synaptic vesicles. **(B)** Amplitude and shape characteristics (10-90% rise time, halfwidth and decay time constant) of spontaneous EPSCs in DKO neurons rescued with Doc2b or GFP as a control.

Figure S4

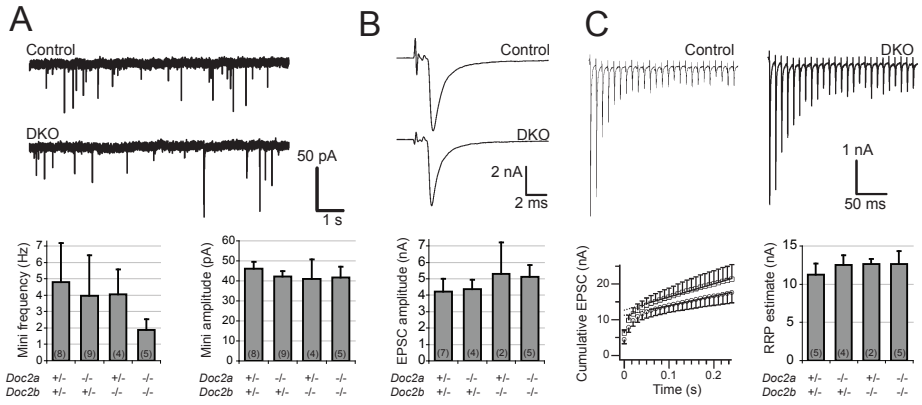

Fig. S4. Neurotransmission at the calyx of Held synapse. **(A)** Whole-cell voltage clamp recordings at the calyx of Held synapse did not reveal significant differences in the frequence or amplitude of miniature events. **(B)** Evoked EPSC amplitude and shape were normal in all groups. **(C)** The size of the ready-releasable pool was normal as estimated by back-extrapolation of the cumulative EPSC during a 100 Hz train.

Figure S5

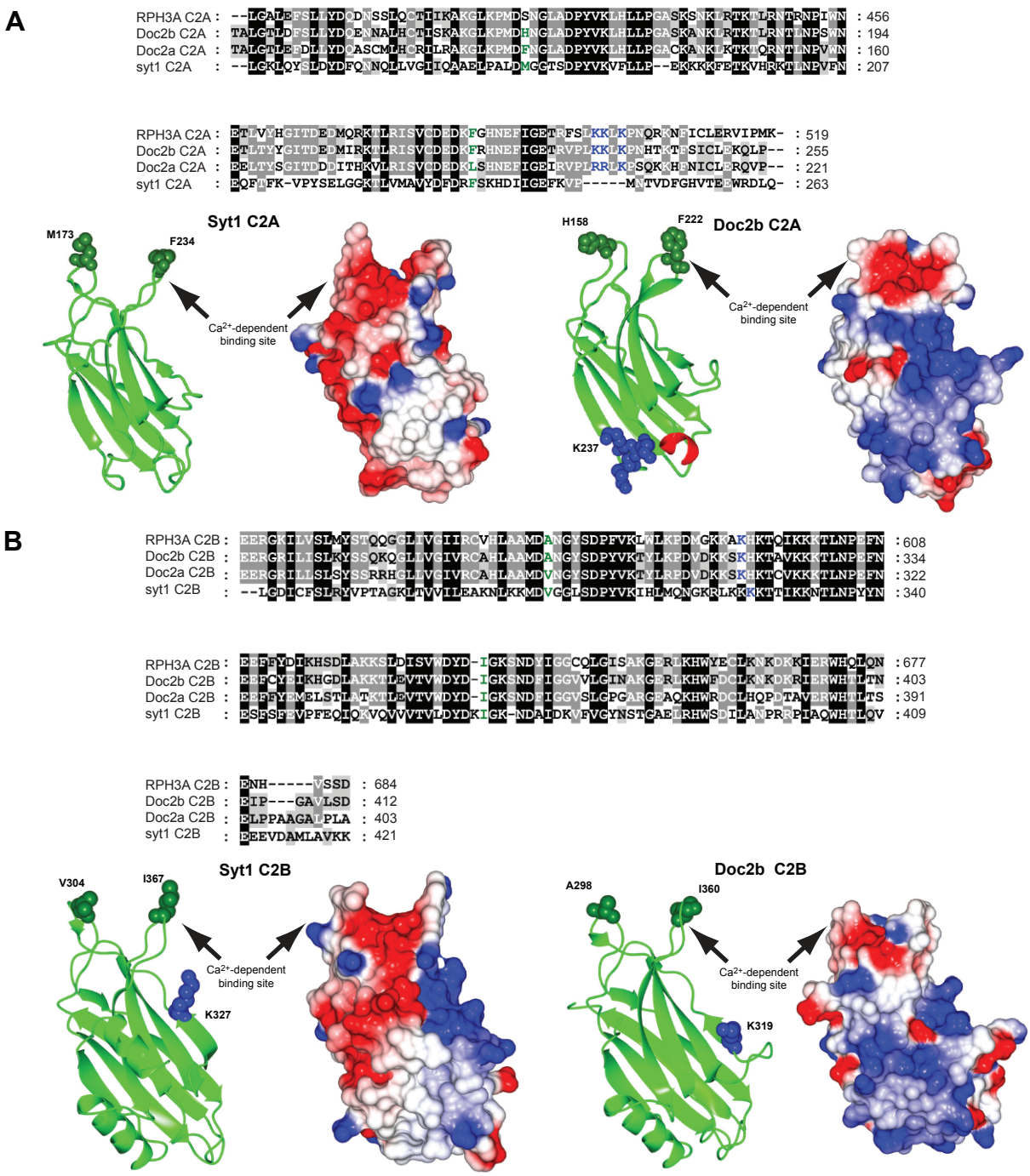

Fig. S5. Structural comparison of C2 domains of Doc2b and synaptotagmin-1. **(A)** Alignment of the C2A domain sequences of human rabphilin3A, rat Doc2b, rat Doc2a and rat synaptotagmin-1. The hydrophobic amino acids at the tip of the Ca^{2+}-binding loops are highlighted in green and the positive amino acids in the insertion of the rabphilin3A, Doc2b and Doc2a C2A domains are highlighted in blue. For the structures of the synaptotagmin-1 and Doc2b C2A domains ribbons (left) and the electrostatic surface potentials (right) are shown. The synaptotagmin-1 C2A domain structure is derived from pdb code 1BYN *(S14)*. The structure of the Doc2b C2A domain was modelled using the rabphilin3A C2A domain (2CHD) *(S12)* as template. The dark green residues represented as "spheres" in the synaptotagmin1 and Doc2b C2A domain structures correspond to the residues highlighted dark green in the alignment. The dark blue residues represented as spheres in the Doc2b C2A domain structure correspond to the dark blue residues in the alignment. **(B)** Alignment of the C2B domains of rat rabphilin3A, rat Doc2b, rat Doc2a and rat synaptotagmin-1 using the same color code as described for the C2A domains in (A). For the structures of the synaptotagmin-1 and Doc2b C2B domains ribbons (left) and the electrostatic surface potentials (right) are shown. The synaptotagmin-1 C2B domain structure is derived from pdb code 1UOW *(S15)*. The structure of the Doc2b C2B domain was modelled using the rabphilin3A C2B domain, pdb 2CM5 *(S13)* as template. The dark blue residues represented as spheres in the Doc2b C2A domain structure correspond to the dark blue residues in the alignment.

Figure S6

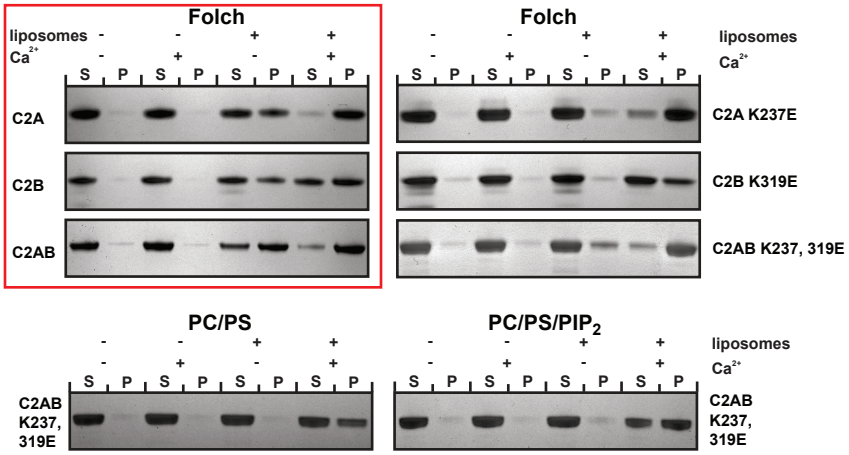

Fig. S6. Identification of the Ca^{2+}-independent membrane binding sites in the Doc2b C2A and C2B domains. Liposome co-sedimentation assay using liposomes of the indicated composition and the indicated Doc2b mutants to analyze the membrane-binding properties of the C2A and C2B domains of Doc2b. The control panel on the left (surrounded by a red box) is reproduced from Fig. 3. The Ca^{2+}-independent binding of the C2A domain to PIP_2-containing and Folch liposomes was surprising as this activity has not been described in the highly homologous C2A domain of synaptotagmin-1. In order to locate the Ca^{2+}-independent PIP_2 binding site in Doc2b we aligned the C2A domain sequences of synaptotagmin-1, Doc2b and the closely related C2A domains of Doc2a and rabphilin3A. The alignment revealed a conspicuous insertion containing the sequence KKLK into the loop connecting beta-strand 7 and 8 (Fig. S5). The mutation K237E (generating the sequence KELK) almost completely abolished Ca^{2+} -independent liposome binding. In the predicted C2 domain structure K237 is located on the opposite site of the Ca^{2+} binding pocket, and may thus allow the Doc2b C2A domain to bind to two membranes simultaneously in the presence of Ca^{2+} (Fig. S5). In order to locate the Ca^{2+}-independent PIP_2 binding site in the C2B domain we mutated K319, located in a polybasic region which is present in many C2 domains including the C2B domain of synaptotagmin-1 *(S11, S16)*. The K319E mutant C2B domain lost Ca^{2+}-independent membrane binding indicating that this site is functionally conserved between synaptotagmin-1 and Doc2b. Consistent with K237 and K319 being involved in Ca^{2+}-independent PIP_2 binding the double mutant Doc2b C2AB fragment almost entirely lost Ca^{2+}-independent binding to Folch liposomes but retained Ca^{2+} -dependent liposome binding (compare to Fig. 3).

Figure S7

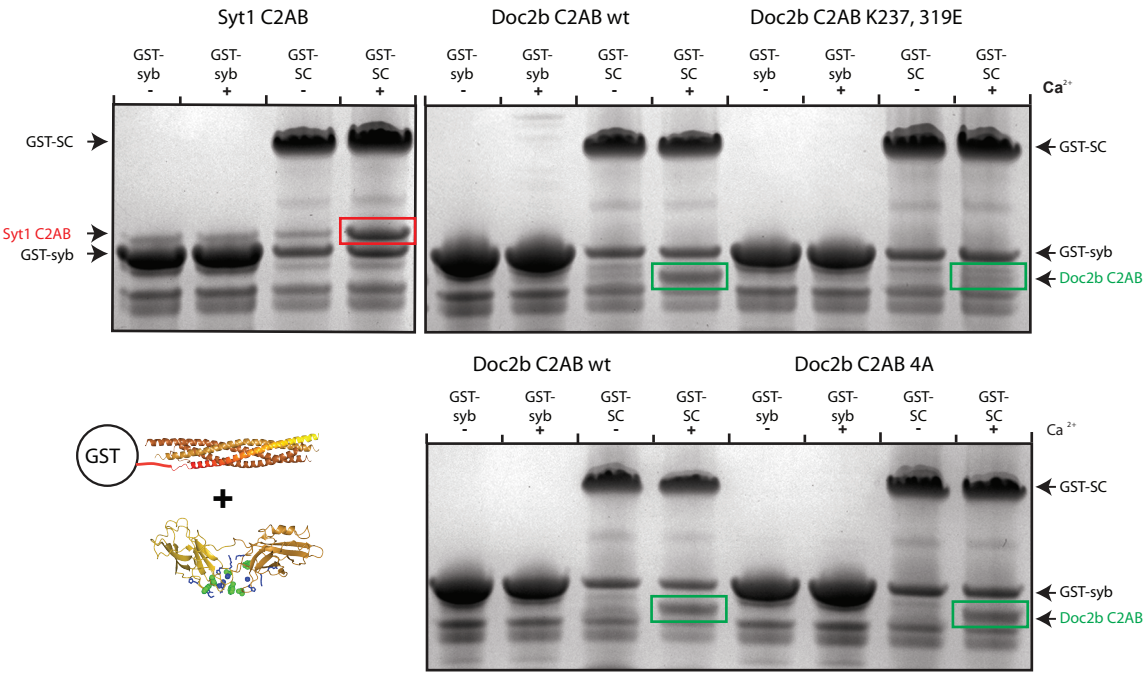

Fig. S7. Pull down experiments using the SNARE complex as bait. 30 µg of the SNARE complex assembled on GST-synaptobrevin (the SNARE domains of SNAP25 and syntaxin-1 did not harbor a N-terminal GST tag) were attached to beads and subsequently incubated with 30 µg of the synaptotagmin C2AB domain, wild-type or mutant Doc2b C2AB domains for 30 minutes at 4°C in the absence (1 mM EDTA) or presence of 1 mM Ca^{2+}. 30 % of the bound material was loaded on 4-12% gradient gels. The gels were stained with Coomassie (the arrows indicate the position of GST-syb: GST-synaptobrevin 1-96, GST-SC: GST-SNARE complex, Syt1: synaptotagmin-1 SC: SNARE complex).

Figure S8

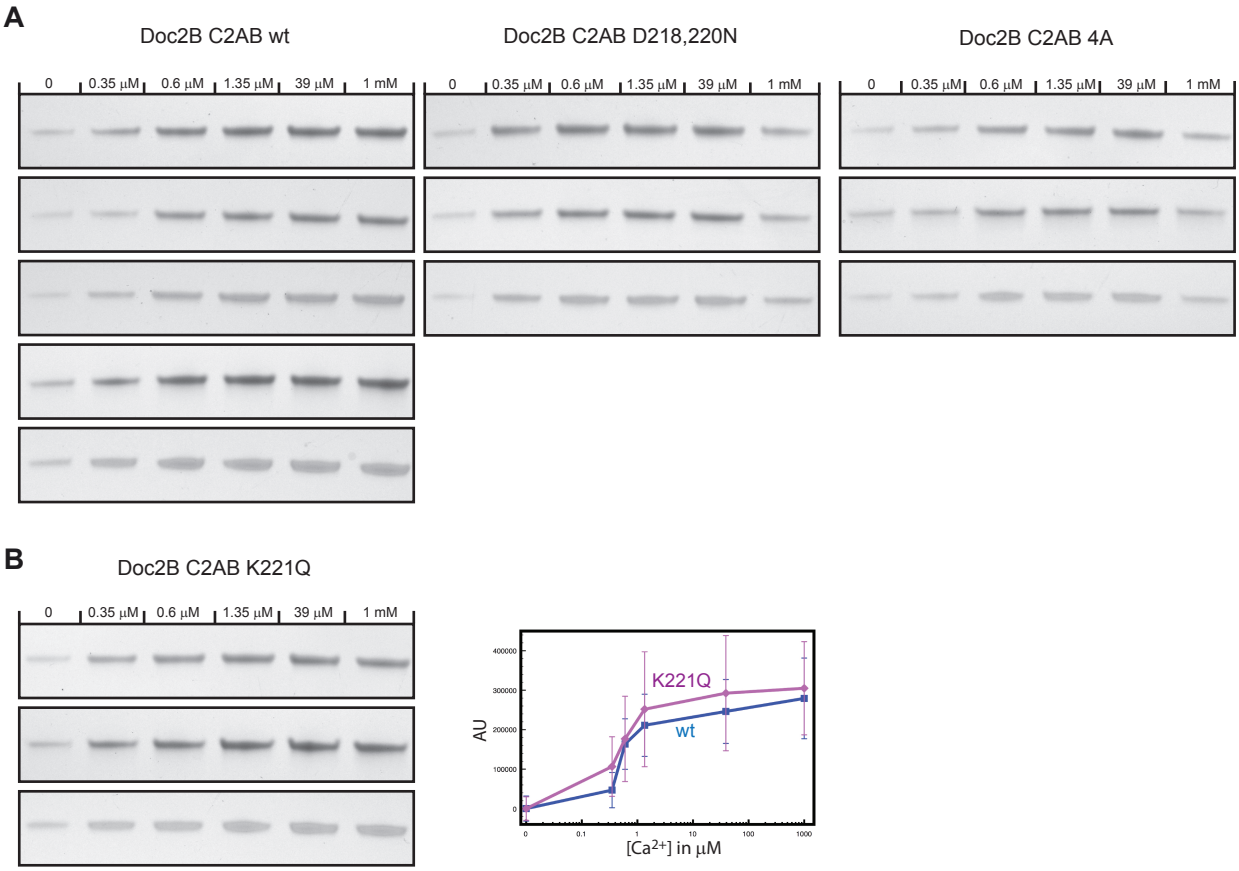

Fig. S8. Ca^{2+}-dependence of liposome co-sedimentation by wild type and mutant Doc2b C2AB. **(A)** Coomassie stained gels of the liposome co-sedimentation assays. The liposomes were composed of 70% PC, 20% PS and 10% cholesterol. At high Ca^{2+} concentrations (1 mM) the extent of liposome-binding by the 4A and D218, 220N mutants were decreased presumably because of unspecific masking of head group charges by the high concentration of divalent cations. **(B)** Liposome binding of K221Q mutant showing no decrease in the Ca^{2+}-dependent binding compared to WT protein (as in panel A) as might be predicted from a similar mutation in synaptotagmin-1 (R233Q) *(S17)*. AU: arbitary units.

Table S1

Figure	Genotype	Expressed protein	[Ca2+]ex	Frequency (Hz)	sem	n (cells)
Fig. 1	Control	none	4 mM	6.23	0.63	169
	DKO	none	4 mM	3.29	0.37	148
		GFP (Semliki)	4 mM	3.06	0.55	46
		Doc2b WT (Semliki)	4 mM	5.49	0.77	54
Fig. 2	Control	none	2 mM	0,71	0,07	28
	Doc2b (-/-)	none	2 mM	0,19	0,02	15
Fig. 5B	DKO	GFP (Lenti)	0.2 mM	1,21	0,15	16
			1 mM	1,69	0,29	21
			2 mM	1,94	0,32	21
			5 mM	4,63	0,61	21
			10 mM	4,68	0,88	20
		Doc2b WT (Lenti)	0.2 mM	2,31	1,12	10
			1 mM	3,84	1,72	10
			2 mM	5,17	2,86	10
			5 mM	8,59	3,46	10
			10 mM	12,94	4,12	9
		Doc2b D218,220N (Lenti)	0.2 mM	9,66	2,48	26
			1 mM	9,53	2,20	26
			2 mM	11,72	2,55	26
			5 mM	16,01	3,05	26
			10 mM	17,08	3,59	25
Fig. 5C	Control	GFP (Lenti)	0.35 mM	0,62	0,15	24
			1 mM	0,93	0,16	34
			5 mM	1,09	0,45	14
			10 mM	2,89	0,56	5
		Doc2b WT (Lenti)	0.35 mM	1,03	0,29	36
			1 mM	1,30	0,40	16
			5 mM	1,81	0,50	17
			10 mM	8,95	1,85	9
		Doc2b D218,220N (Lenti)	0.35 mM	2,70	0,54	34
			1 mM	3,11	0,74	33
			5 mM	3,87	0,80	20
			10 mM	9,20	3,59	7
Fig. 5D	DKO	Doc2b WT (Lenti)	0.2 mM	2,48	0,44	34
			1 mM	2,87	0,54	34
			2 mM	4,01	1,10	34
			5 mM	5,81	0,00	34
			10 mM	11,00	0,00	31
		Doc2b K237,319E (lenti)	0.2 mM	1,70	0,36	31
			1 mM	1,77	0,35	30
			2 mM	2,43	0,35	31
			5 mM	3,48	0,68	31
			10 mM	5,28	1,12	25

Table S1. Overview of spontaneous release frequencies measured in hippocampal autapses and Purkinje cells. Data from Fig. 1 (autapses), Fig. 2 (cerebellar Purkinje cells) and Fig. 5 (network cultures) are listed together with their experimental parameters, mean values, standard errors and cell numbers.

REFERENCES

S1. A. J. Groffen *et al.*, *J Biol Chem* **279**, 23740 (2004).
S2. A. Maximov, O. H. Shin, X. Liu, T. C. Sudhof, *J Cell Biol* **176**, 113 (2007).
S3. A. J. Groffen, L. Jacobsen, D. Schut, M. Verhage, *J Neurochem* **92**, 554 (2005).
S4. G. Sakaguchi *et al.*, *The European journal of neuroscience* **11**, 4262 (1999).
S5. K. D. Wierda, R. F. Toonen, H. de Wit, A. B. Brussaard, M. Verhage, *Neuron* **54**, 275 (2007).
S6. Y. Otsu *et al.*, *J Neurosci* **24**, 420 (2004).
S7. J. Xu, Z. P. Pang, O. H. Shin, T. C. Sudhof, *Nat Neurosci* **12**, 759 (2009).
S8. A. Fisyunov, V. Tsintsadze, R. Min, N. Burnashev, N. Lozovaya, *J Neurophysiol* **96**, 1267 (2006).
S9. R. L. Habets, J. G. Borst, *J Physiol* **564**, 173 (2005).
S10. R. Friedrich *et al.*, *J Neurosci* **28**, 6794 (2008).
S11. S. Martens, M. M. Kozlov, H. T. McMahon, *Science* **316**, 1205 (2007).
S12. M. Biadene, P. Montaville, G. M. Sheldrick, S. Becker, *Acta Crystallogr D Biol Crystallogr* **62**, 793 (2006).
S13. P. Montaville *et al.*, *J Biol Chem* **282**, 5015 (2007).
S14. X. Shao, I. Fernandez, T. C. Sudhof, J. Rizo, *Biochemistry* **37**, 16106 (1998).
S15. Y. Cheng *et al.*, *Protein Sci* **13**, 2665 (2004).
S16. J. Bai, W. C. Tucker, E. R. Chapman, *Nat Struct Mol Biol* **11**, 36 (2004).
S17. R. Fernandez-Chacon *et al.*, *Nature* **410**, 41 (2001).